Biomedicine & Pharmacotherapy 202 (2026) 119770

Contents lists available at ScienceDirect

Biomedicine & Pharmacotherapy

journal homepage: www.elsevier.com/locate/biopha

Steroid-loaded Avidin-Nucleic-Acid-Nano-Assemblies reduce hepatic fibrosis modulating Kupffer cells in primary biliary cholangitis

Martina Bruna Violatto [a,*], Manuela Vitulo [b], Elisa Schiavon [c], Chiara Caime [b], Annalisa Morelli [a], Martina Cattaneo [a], Naths Grazia Sukubo [b], Mara Corti [a], Giulia Yuri Moscatiello [a], Alessandro Enrico Galbussera [a], Alice Passoni [d], Alessia Lanno [d], Stefano Fumagalli [e], Davide Panzeri [f], Laura Sironi [f], Martina Stocco [c], Simone Bernardotto [c], Domenico Cerullo [g], Laura Cristoferi [h], Alessio Gerussi [b,h], Sara Pelucchi [b], Massimiliano Cadamuro [b], Marco Carbone [b,i], Pietro Invernizzi [b,h,**], Paolo Bigini [a], Margherita Morpurgo [c], Donatella Barisani [b,h]

[a] Department of Biochemistry and Molecular Pharmacology, Istituto di Ricerche Farmacologiche "Mario Negri" IRCCS, Milano, Italy
[b] Department of Medicine and Surgery, University of Milano Bicocca, Monza, Italy
[c] Department of Pharmaceutical and Pharmacological Sciences, University of Padova, Padova, Italy
[d] Department of Environmental Health Sciences, Istituto di Ricerche Farmacologiche "Mario Negri" IRCCS, Milano, Italy
[e] Department of Acute Brain and Cardiovascular Injury, Istituto di Ricerche Farmacologiche "Mario Negri" IRCCS, Milano, Italy
[f] Department of Physics, University of Milano Bicocca, Milano, Italy
[g] Department of Molecular Medicine, Istituto di Ricerche Farmacologiche "Mario Negri" IRCCS, Centro Anna Maria Astori Science and Technology Park Kilometro Rosso, Bergamo, Italy
[h] Division of Gastroenterology, Center for Autoimmune Liver Diseases, European Reference Network on Hepatological Diseases (ERN RARE-LIVER), IRCCS Fondazione San Gerardo dei Tintori, Monza, Italy
[i] Hepatology and Gastroenterology, ASST Grande Ospedale Metropolitano Niguarda, Milano, Italy

ARTICLE INFO

Keywords:
Autoimmune liver disease
Corticosteroids
Nanoparticles
Hepatic macrophages
Targeted drug release

ABSTRACT

Primary biliary cholangitis (PBC) is the most common life-long autoimmune liver disease arising from a biliary epithelial activation to a complex evolving cascade of immune-mediated injury, leading to inflammation and fibrosis and ultimately cirrhosis and liver failure. Ursodeoxycholic acid (UDCA) remains the only first-line treatment, despite being ineffective in approximately 40% of patients. Inadequate response to UDCA has been associated with increased death risk or need for liver transplantation. Starting from these premises, novel or repurposed drugs are currently needed. Immunosuppressive therapies, such as corticosteroids, remain controversial, primarily due to safety concerns related to off-target effects and limited evidence of enhanced efficacy.

Nanoparticles are known to accumulate in the liver. Among them, Avidin-Nucleic-Acids-Nano-ASsemblies (ANANAS) have emerged as promising drug carriers thanks to their multi-functionality and convenient tunability, biodegradability, biocompatibility and scalable manufacturing.

Despite the availability of numerous PBC models, none replicate key features of human disease to the degree observed in ARE Del-/- mice. Focusing on this model, ANANAS loaded with acid-releasable dexamethasone (ANANAS-Hz-Dex-M) were parenterally administered to evaluate distribution, pharmacokinetics, and therapeutic efficacy.

The single treatment demonstrated selective liver tropism with an exclusive steroid release, and interaction with resident macrophages. Multiple administrations significantly reduced hepatic fibrosis. *In vitro*, isolated Kupffer cells from ARE Del-/- internalize the nanoassembly, with a reduction of the inflammatory profile.

Our findings delineate ANANAS-Hz-Dex-M as a tool with the potential to guide resident macrophage plasticity and ameliorate disease course.

* Correspondence to: Laboratory of Nanobiology and Nanotoxicology, Italy.
** Correspondence to: Fondazione IRCCS San Gerardo dei Tintori, Monza, Italy.
E-mail addresses: martina.violatto@marionegri.it (M.B. Violatto), pietro.invernizzi@unimib.it (P. Invernizzi).

https://doi.org/10.1016/j.biopha.2026.119770
Received 10 July 2026; Accepted 14 July 2026
Available online 22 July 2026

1. Introduction

Primary biliary cholangitis (PBC) is a chronic autoimmune liver disease characterized by the progressive destruction of small intrahepatic bile ducts, leading to chronic cholestasis, fibrosis, and cirrhosis. It is diagnosed by the presence of chronic cholestasis and anti-mitochondrial or anti-nuclear antibodies; in patients undergoing liver biopsy, granulomatous lymphocytic cholangitis can be evident [1,2]. Ursodeoxycholic acid (UDCA) is the standard treatment [3], but it is ineffective in up to 40% of patients, who require additional treatment [4–8].

In addition PBC can overlap with another autoimmune liver disease, i.e. autoimmune hepatitis (AIH) approximately in 10% of patients with either AIH or PBC [9,10], and approximately 30% of patients with PBC have at least one extrahepatic autoimmune (EHA) conditions condition [11]. These conditions require immune response suppression, and both corticosteroids and immunosuppressants are prescribed for this purpose. Several clinical studies investigating the combination of UDCA with corticosteroids for PBC treatment have been published [6,12,13]. These studies indicate a moderate to marked improvement in some biochemical markers of liver function in patients treated with combination therapy, even if long-term corticosteroid side effects are evident.

Nanotechnology offers a promising solution by enhancing drug bioavailability, and targeting specificity, thereby reducing systemic side effects [14]. Nanoparticles (NPs) can improve drug delivery by accumulating and persisting in the liver after systemic administration, interacting primarily with non-parenchymal hepatic cells such as Kupffer cells (KCs) and liver sinusoidal endothelial cells (LSECs) [15–17].

Among the various nanocarriers, polyavidin-based Avidin-Nucleic-Acids-Nano-ASsemblies (ANANAS) have shown potential as a multifunctional, biodegradable, and biocompatible drug delivery system [18]. Our previous studies demonstrated the effectiveness of ANANAS in delivering the therapeutic compounds to the liver in a murine model of AIH, and also the localization of the particles in the KCs [19]. This localization, in particular for ANANAS loaded with dexamethasone (ANANAS-Hz-Dex), could be important in the regulation of KC function which, in turn, could affect the pathogenetic processes in PBC. The importance of KCs has been recently demonstrated by various studies [20], including a single cell study, which demonstrated that an enhanced proinflammatory roles of these cells may increase the local inflammatory response in the liver [21].

The present study evaluated the therapeutic potential of the ANANAS-Hz-Dex formulation in a recently developed murine model of PBC, the ARE-Del-/- mouse, which exhibits key aspects of human PBC, including female predominance, autoimmune cholangitis, portal inflammation, and hepatic granulomas [22,23].

Our approach involved a detailed characterization of the ARE-Del-/- model, and an evaluation of the new generation ANANAS-Hz-Dex-M in two lines of treatment: a single administration to assess carrier biodistribution and steroid pharmacokinetics, and a multiple one to evaluate therapeutic effects on hepatic inflammation and fibrosis.

2. Materials and methods

2.1. Preparation of ANANAS-Hz-Dex-M

The ANANAS-Hz-Dex-M formulation was obtained as described by Morelli et al. [24]. Briefly, empty (core) ANANAS, previously obtained in freeze-dried form [18,25], were dissolved in phosphate buffer containing stoichiometrically controlled amounts of the desired long-(5 kDa poly(ethylene glycol-PEG) - and short-spaced biotin-Hz-Dex conjugates. The long-spaced derivative was added to cover 25% of the total biotin binding sites (BBS); the short-spaced one was added to cover 40% of the BBS. Preformulation studies [24] had shown that at these biotin:BBS ratios, both biotin conjugates are fully retained by the NPs so that no purification is necessary after reconstitution. In these assemblies [19,24,26], dexamethasone is reversibly tethered via a hydrazine bond that is stable at neutral pH but hydrolysed in acidic pH. The mixtures were allowed to stand for at least 1 h prior to use and were administered within one day after preparation.

Fluorescently labeled ANANAS-Hz-Dex-M (F-ANANAS-Hz-Dex-M) for the single treatment were obtained by adding biotin-C6-Alex633 to the assembly mixture to cover 5% of the total BBS, at the detriment of the short-spaced biotin-Dex conjugate.

Drug-free ANANAS were obtained following the same protocol by resuspending core NPs with a titrated 5 kDa α, biotin, ω-methoxy-poly (ethylene glycol) (Laysan Bio, Huntsville, AL- USA), which was added at a total 25% BBS coverage.

2.2. Animals

The Institute for Pharmacological Research Mario Negri IRCCS adheres to the principles governing the care and use of laboratory animals established by: Italian Law (D.lgs 26/2014; authorisation no. 19/2008-A issued March 6, 2008 by Ministry of Health); Mario Negri Institutional Regulations and Policies (Quality Management System Certificate-UNI EN ISO 9001:2015-Reg. no. 6121); the NIH Guide for the Care and Use of Laboratory Animals and EU directives and guidelines (EEC Council Directive 2010/63/UE). In the present work, we used a transgenic mouse model, the ARE-Del-/-, which was kindly provided by Professor Young H.A. (NIH, Bethesda) characterized by chronic expression of the IFN-γ gene that mimics some key aspects of human PBC. The animal studies were approved by the Mario Negri Institute Animal Care and Use Committee (IACUC) and by the Italian National Institute of Health (code no. 58/2020-PR). The animals were kept under specific pathogen-free conditions in the Institute's animal care facilities in rooms with a constant temperature of $21 \pm 1°C$, humidity of $55 \pm 10\%$, a 12-h light-dark cycle, and ad libitum access to food and water. The animal diet is composed of wheat, extruded soybeans, barley, wheat bran, soybean meal produced from genetically modified soybeans, calcium carbonate, dicalcium phosphate, sodium chloride, vitamins and minerals. For animal welfare, bedding and environmental enrichment, such as a "mouse house", are available. The mice were regularly checked by a veterinarian responsible for monitoring animal welfare. In our animal cohort, the ARE-Del-/- mutation was associated with a higher female mortality; indeed, we assessed 33% mortality from weaning to 20 weeks of age before treatment initiation, whereas it was to 2% in males.

2.3. In vivo treatments

Characterization study: Wild-type (WT) and ARE-Del-/- (HO) sibling littermate mice, both males and females, were monitored for body weight without any treatment. At 20 and 24 weeks of age, mice were anaesthetized, blood was collected via retroorbital bleeding, and serum was analysed. After sacrifice, the livers were collected, fixed in 10% neutral buffered formalin (Bio-Optica, Italy) for 24 h, and embedded in paraffin for immunohistochemistry or frozen for immunofluorescence or molecular analyses.

Single-dose treatment study: thirty-five WT mice at 20 weeks of age were enrolled and intraperitoneally (i.p.) injected with free dexamethasone (Dex) (0.167 mg/kg; $n = 16$) or F-ANANAS-Hz-Dex-M (11.4 mg/kg of NPs loaded with 0.167 mg/kg of Dex; $n = 16$). The remaining three mice were treated with PBS and used as controls. In parallel, 32 HO mice at 20 weeks of age were i.p. injected with free Dex (0.167 mg/kg; ($n = 16$) or F-ANANAS-Hz-Dex-M (11.4 mg/kg of NPs loaded with 0.167 mg/kg of Dex; $n = 16$). Both WT and HO mice were euthanized at 30 min, 4, 24, and 48 h after treatment ($n = 4$ for each time point). The plasma, liver, lung, kidney, spleen and brain were collected for *ex vivo* imaging and frozen for biodistribution and pharmacokinetics.

Multiple-dose treatment study: fourteen HO male mice at 20 weeks of

age were included in the study. They were randomly assigned to free Dex (0.167 mg/kg; n = 6), ANANAS (10.54 mg/kg; n = 4) or ANANAS-Hz-Dex-M treatment (10.54 mg/kg of NPs loaded with 0.167 mg/kg of Dex; n = 4). Their body weight was assessed over time. The animals received nine serial i.p. injections (3 per week for 3 weeks). At sacrifice, the mice were anesthetised, blood was collected and serum was analysed. Livers were fixed in 10% neutral buffered formalin for 24 h and embedded in paraffin for immunohistochemistry or frozen for immunofluorescence, molecular analyses, or ELISA on tissue homogenates.

2.4. Ex vivo fluorescence imaging

Ex vivo optical imaging was performed on excised organs (liver, lung, spleen, kidneys, and brain for WT mice, and exclusively liver for HO mice) at 30 min, 4, 24 and 48 h after treatment, using the IVIS Lumina III imaging system (PerkinElmer). The following parameters were used: excitation filter range 680–740 nm, emission filter (790 nm, exposure time 2 s), binning factor 4, and f/Stop 2. Image processing and analysis were performed using Living Image 4.3.1 software.

2.5. Anti-mitochondrial antibodies (AMA) detection

AMA levels were measured using a commercial ELISA kit (code MBS7207392; MyBioSource, USA) in samples (n = 3 per experimental group) obtained from the multiple-dose treatment study. Undiluted liver homogenates were analyzed according to the manufacturer's instructions. Optical density (OD) was measured at 450 nm using a Tecan Infinite 200 Pro microplate reader (Männedorf, Switzerland). All samples were assayed in duplicate. AMA concentrations were determined from the standard curve and expressed as ng/mL.

2.6. Serum biochemical analysis

Alkaline phosphatase (ALP, U/L) and total bile acids (TBA, μmol/L) were measured in 100 μL serum samples using the liver rotor through the Element Rc analyser (Antech Diagnostics Italy S.r.l., Treviglio, Italy).

2.7. Immunohistochemistry

Liver sections (4 μm) were cut with Leica RM55 microtome (Leica Microsystems, Italy). Slices were deparaffinised in xylene and rehydrated through a series of alcohols in water. Hematoxylin and eosin (HE) staining was performed as previously described [27]. IBA−1 staining (1:500, Wako Chemicals, USA) was performed to provide an overview of macrophage infiltration. Antigen retrieval was performed with citrate buffer (pH 6) for 30 min at 95°C, endogenous peroxidase activity was inhibited with 3% H_2O_2 for 10 min at RT, and incubation with blocking solution (PBS-NGS 10%-Tween20 0.05%) was carried out for 30 min at RT. Sections were assayed using Vectastain Elite ABC (Vector Laboratories, Burlingame, CA, USA) and stained with 3,3-Diaminobenzidine (DAB, Sigma-Aldrich). To assess fibrosis, the collagen fibres were stained with Picro-Sirius Red solution (Bio-Optica, Italy) for 1 h and washed with acidified water. The slides were observed via Virtual Slide Microscopy (Olympus, Japan); the percentages of the area occupied by cellular infiltrated (HE) and by macrophages (IBA−1) were determined using ImageJ software. The slides were also processed through QuPath software to obtain five 3000 × 3000 px fields per mouse and ImageJ software was used to measure the average size (μm^2) and the Feret diameter (μm) of the IBA−1 positive macrophages.

2.8. Segmentation and quantification of collagen in Sirius Red WSIs

Whole-slide images (WSIs) were converted from the proprietary VSI Olympus file format to an RGB pyramidal OME-TIFF image with QuPath software [28]. Their following processing was handled through custom MATLAB scripts employing the Blocked Processing Toolbox, which enhances operations on tiled and pyramidal images. Sirius Red stained WSIs were analysed as previously described [29]. In brief, RGB data were converted into optical density (OD) space and collagen was segmented by using stain vector deconvolution and Otsu's thresholding on the Sirius Red stain channel. Quantitative features such as the "Collagen Area", which describes the fraction of collagen pixels (Sirius Red positive) over the total number of pixels representing the tissue section, and the "Entropy of Collagen", a textural parameter encoding randomness of values in 32 × 32 pixel ROIs were extracted. The contribution of Glisson's collagen capsule was removed from all the quantifications.

2.9. Immunofluorescence

To detect macrophages, immunofluorescence analysis for CD68 antibody was performed on liver sections from the single-dose treatment. Tissue slides (10 μm thick) were cut by cryostat, fixed in 10% neutral buffered formalin for 20 min, washed with phosphate-buffered saline (PBS), and incubated for 1 h with a blocking solution (PBS-NGS 10% - TritonX−100 0.1%). Anti-CD68 (1:200, Bio-Rad Laboratories, USA) + TritonX−100 0.1% + NGS 3% in PBS O/N at 4°C was used. After washing, sections were incubated with the secondary alexa488-conjugated antibody (1:500, Invitrogen Thermo Fisher Scientific, USA) for 1 h at RT in a 1% PBS-NGS solution. Nuclei were stained with Hoechst−33258 (2 μg/mL, for 10 min). Specific lasers λexc 405 nm, 488 nm, and 640 nm, were used to visualize the signals related to Hoechst−33258 (nuclei), Alexa488 (CD68) and Alexa633 (ANANAS), respectively. Samples were acquired using Nikon A1 confocal microscope.

To evaluate NF-kB localization in macrophages, immunofluorescence analysis was performed on liver sections obtained from the multiple-dose treatment study. Tissue sections (14 μm thick) were cut by cryostat, post-fixed in 10% neutral buffered formalin for 20 min, washed with PBS, and incubated for 1 h with a blocking solution (PBS-NGS 5% - TritonX−100 0.3%). Macrophages were identified using an anti-CD68 antibody, as described above. The primary antibody against NF-kB p65 (1:200, Cell Signaling Technology, USA) was diluted in TritonX−100 0.3% + NGS 3% in PBS and incubated O/N at 4°C. After washing, sections were incubated for 1 h at RT in PBS + TritonX−100 0.3% + NGS 3% with Alexa Fluor 488-conjugated and Alexa Fluor 546-conjugated secondary antibodies (both 1:500, Invitrogen Thermo Fisher Scientific, USA) for the detection of CD68 and NF-kB, respectively. Nuclei were stained with Hoechst−33258 (2 μg/mL, for 10 min). Specific lasers at λ_{exc} 405, 488, and 640 nm, were used to visualize the signals related to Hoechst−33258 (nuclei), Alexa488 (CD68) and Alexa546 (NF-kB), respectively. Samples were acquired using Olympus IX71 fluorescence microscope and four fields per experimental group were captured using a 40 × objective. Image analysis was performed using an originally-developed macro on ImageJ software. Briefly, CD68-positive cells were identified and their nuclei segmented with the Moments method. The resulting binary image was used to generate a mask, which was subsequently applied to the NF-kB channel to quantify fluorescence intensity. NF-kB nuclear presence was expressed as the sum of nuclear NF-kB-positive pixels (raw integrated density).

2.10. Pharmacokinetics

The internal standard fludrocortisone (10 ng) was added to samples from treated mice, and Dex (0–300 ng) and fludrocortisone (10 ng) were included in the calibration curve. Liver and kidney pieces were digested with methanol (1:2 w/v) and acetonitrile (1:1 w/v), stirred and sonicated for 20 min. Water (1:10 w/v) was then added, and the stirring and sonication steps were repeated; the samples were subsequently centrifuged at 7000 ×g for 15 min at 4°C. The supernatant was cleaned up via solid-phase extraction using Sep-Pak C18 1 cc Vac Cartridges (Waters, Milford, MA, USA), which were preconditioned with methanol, followed

by water. The samples were loaded onto SPE columns; the cartridges were rinsed with water: acetone (80:20) and then with water before being dried under vacuum for 5 min. The samples were eluted with acetonitrile. The plasma aliquots were eluted with acetonitrile (1:4 v/v) and centrifuged at 7000 ×g for 15 min at 4°C. All samples were evaporated and suspended in 100 μL of 0.05% acetic acid: acetonitrile (80:20).

High-performance liquid chromatography (HPLC) and tandem mass spectrometry (MS/MS) were performed. The LC-MS/MS system was a Nexera ultrahigh-pressure liquid chromatography (UHPLC) system interfaced with a triple quadrupole LCMS−8060 (Shimadzu, Japan). The mass spectrometer (MS) was operated in negative electrospray ionization (ESI) mode, following the experimental conditions already reported [26].

2.11. Gene expression analysis

RNA was extracted from the livers of chronically treated ARE-Del-/- mice using the Quick RNA Kit (Zymo Research, Irvine, CA). RNA quality and quantification were performed using a NanoDrop 1000 spectrophotometer (Applied Biosystems, Thermo Fisher Scientific, Waltham, MA, USA). cDNAs were synthesized from RNA samples using the High-Capacity cDNA Reverse Transcription Kit (Applied Biosystems™, Thermo Fisher Scientific, Waltham, MA, USA). Quantitative PCR (qPCR) was performed using TB Green Premix Ex-Taq (Takara, Diatek Lab Line, Jesi, Italy) on Quant Studio 7 Flex (Applied Biosystems™, Thermo Fisher Scientific, Waltham, MA, USA), and CXR (ROX) was selected as a passive reference dye. The employed primers are described in the Table S1, Supplementary Material. The HPRT housekeeping gene was used for data normalization and the 2-ΔΔCt method was used for relative expression using an external calibrator.

2.12. In vitro treatment

KCs were isolated from the livers of WT and HO mice at 24 weeks of age [27,30]. After euthanasia, the livers were perfused in situ with sterile PBS and then enzymatically digested in RPMI medium containing collagenase IV (200 U/mL; Sigma-Aldrich) and DNase I (100 U/mL; Sigma-Aldrich) for 30 min at 37°C. Following digestion, the tissue was mechanically homogenized and filtered to generate a single-cell suspension. Hepatocytes were separated from non-parenchymal cells (NPCs) via low-speed centrifugation at 400 rpm for 6 min. To isolate KCs, the NPC fraction was plated on 6-well plates at a density of 1, 5×10^7 cells/well in Dulbecco's modified eagle medium (DMEM) with 10% fetal bovine serum (FBS) and 1% penicillin-streptomycin. After 2 h of incubation at 37°C, non-adherent cells were removed. Adherent KCs were treated with either vehicle (control), Dex (3.17 μg/mL), ANANAS (200 μg/mL), or ANANAS-Hz-Dex in complete DMEM containing 50 ng/mL M-CSF for 24 h. The cells were then harvested for gene expression analysis. Real-time qPCR analysis was performed using Fast SYBR™ Green Master Mix (Applied Biosystems), with a QuantStudio™ 5 Real-Time PCR System (Applied Biosystems). The HPRT1 gene was used for the normalization using the ΔCt method. The data are expressed as Log_2 of Fold changes.

2.13. Statistics

Statistical analyses were performed using GraphPad Prism Software 11.0.2 (San Diego, CA, USA). Grubb's test was used to assess the presence of outliers within each group. One-way ANOVA followed by uncorrected Fisher's LSD or by Tukey post-hoc tests was used to compare the groups of interest during *in vivo* or *ex vivo* experiments. For *in vitro* test, two-way ANOVA followed by Tukey post-hoc test was selected.

3. Results

3.1. Increased inflammation and fibrosis in ARE-Del-/- mouse model

Compared with wild-type (WT) controls, ARE-Del-/- (HO) mice presented significantly lower body weights, with a more pronounced effect in females (Fig. 1A). Conversely, the spleen weight was higher in HO mice compared to WT mice, which could indicate increased immune function and congestion (Fig. 1B) [31,32]. Elevated levels of serum alkaline phosphatase (ALP) and total bile acids (TBA) in HO mice confirmed the presence of cholestasis (Fig. 1C-D), supporting the reliability of this murine model of PBC [33]. The increase in TBA (typically found in patients with obstructive jaundice or cholestasis) observed by Bae H.R. at 8 and 20 weeks of age [23] was also validated by our study at 24 weeks of age.

Histopathological examination of liver sections from ARE-Del-/- mice (HO) revealed significantly greater cellular infiltration and fibrosis compared to WT controls (Figs. 2 and 3). HE staining revealed perivascular inflammatory foci, particularly in females and older mice, whereas WT mice showed no inflammation or damage (Fig. 2A-C). IBA−1 staining, a marker of activated macrophages indicated an increase in macrophage infiltration and an alteration in their morphology, larger and more elongated, in HO mice (Fig. 2B-D).

Sirius Red staining highlighted extensive fibrosis with evident collagen deposition in both perivascular and perisinusoidal regions (Fig. 3A-B) in HO mice, compared to controls. Quantitative analyses confirmed a significant increase in the collagen content in HO mice compared to controls, and a trend toward a progressive increase in the collagen area in HO mice over time. In addition, we detected a decrease in entropy in HO mice from 20 to 24 weeks of age, indicating the presence of more organized fibrosis (Fig. 3C-D) [34,35].

Gene expression analysis further characterized the PBC model (Fig. 4). Compared with WT control mice, HO mice exhibited significant upregulation of inflammatory cytokines (IFN-γ, IL-1β, TNF-α, and CCL2) and these variations were age- and sex-dependent (Fig. 4A). Although TGF-β induction was not statistically significant in all experimental groups, it was higher in HO animals compared to WT, supporting its role in triggering fibrosis. The fibrotic process was confirmed by the upregulation of fibrotic markers (α-SMA, COL1α1, COL1α2, COL3α1, MMP2, MMP9, and TIMP1) in HO mice (Fig. 4B). The α-SMA gene, a marker of activated stellate cells, was significantly upregulated exclusively in HO male mice at 24 weeks, with no significant changes in HO female mice. Collagen genes (COL1α1, COL1α2 and COL3α1) were also elevated in HO mice compared with WT mice, with a peculiar trend of each type depending on mouse age and sex. In particular, the level of collagen 1α1, a major component of extracellular matrix proteins [36], was increased in HO female mice at 24 weeks, whereas the level of collagen 3α1, which is involved in scar formation [37], was significantly higher in HO male mice at 24 weeks. Furthermore, a significant increase in the mRNA levels of MMP9 and TIMP1, which are involved in matrix remodeling, was detected in HO animals.

3.2. Single ANANAS-Hz-Dex-M treatment exhibits hepatic tropism and selective drug release

The biodistribution and pharmacokinetics of ANANAS-Hz-Dex-M, fluorescently labeled with Alexa633 dye, were investigated in WT and HO mice to evaluate changes in the liver undergoing inflammation and fibrosis (Fig. 5). *Ex vivo* optical imaging of WT mice showed that i.p. injected F-ANANAS-Hz-Dex-M exhibited hepatic tropism (Fig. 5A) with minimal signals in off-target organs (Figure S1, SI). Specifically, at the first two time points (30 min and 4 h), the signal associated with ANANAS was detectable in all selected organs (liver, lungs, kidneys, and spleen) except the brain, likely due to blood circulation. However, one day after treatment, the fluorescence pattern showed almost exclusive tropism toward the liver.

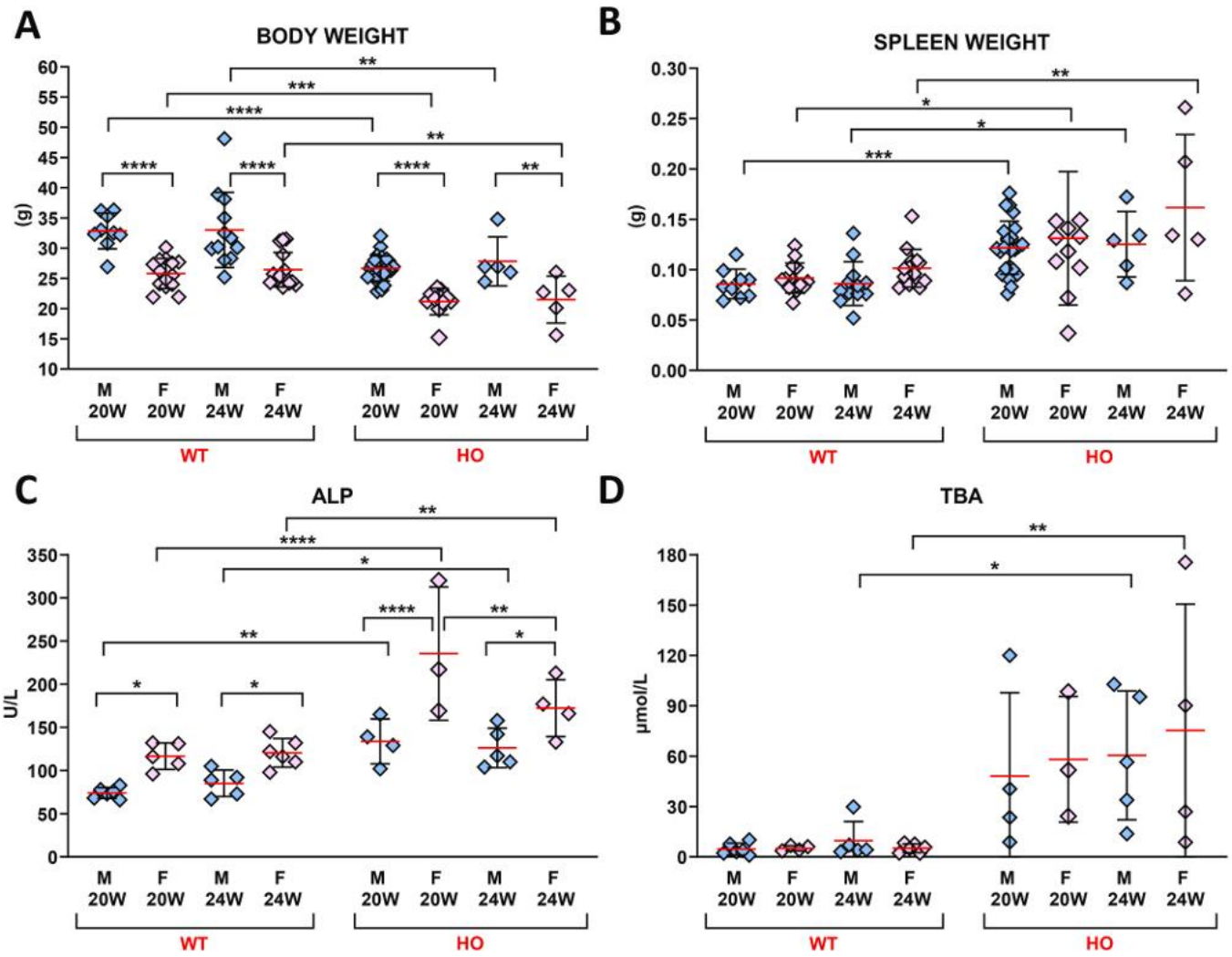

Fig. 1. ARE-Del-/- mouse model general characterization. A) body weight, B) spleen weight, C) serum alkaline phosphatase (ALP) and D) serum total bile acids (TBA) levels were reported. Male (M) and female (F) healthy (WT) and ARE-Del-/- (HO) mice at 20 and 24 weeks of age were included in the study. Data are presented as a scatter plot, reporting mean + /- SD. Statistical analysis is performed by One-way ANOVA, followed by Fisher's LSD test. *$p < 0.1$, **$p < 0.01$, ***$p < 0.001$, ****$p < 0.0001$.

The ability of F-ANANAS-Hz-Dex-M to localize in the liver was also confirmed in HO mice, even if significant differences with WT mice were observed in terms of the kinetics and accumulation rate of the NPs. In HO mice, the NPs penetrated the liver more slowly, reaching the maximum concentration at 4 h and remaining constant until 24 h. Notably, the number of NPs in the liver was higher compared to WT mice as detected by ANANAS fluorescence measurements (Fig. 5A). This latter result can be explained by macrophage hypertrophy in HO mice, resulting in a higher surface area available for ANANAS phagocytosis (Fig. 2B-D).

Immunofluorescence analysis of liver tissues using an anti-CD68 antibody confirmed the efficient interaction and colocalization of F-ANANAS-Hz-Dex-M with hepatic macrophages in both WT and HO conditions (Fig. 5B). Four hours after treatment, F-ANANAS-Hz-Dex-M (red signal) efficiently colocalized (yellow spots) with the macrophages (green signal). Our data align with results in the literature that attribute KCs as the main cells involved in hepatic uptake [15].

Pharmacokinetic studies (Fig. 5C) in livers from WT mice (blue lines) showed higher levels of Dex released from F-ANANAS-Hz-Dex-M than from the free drug alone 4 h after administration, and this release persisted over time (up to 48 h). Selective drug release from NPs in the liver was also maintained in HO mice (red lines), with Dex levels remaining relatively constant between 4 and 24 h. Consistent with the previous F-ANANAS-Hz-Dex formulations, no dexamethasone was released from the NPs in plasma or off-target organs [19,26].

Gene expression analyses were performed on liver samples from HO mice, with a focus on acute-phase cytokine genes (Figure S2, SI). Collectively, these data show that free Dex more quickly reduces the mRNA levels of these cytokines (mainly at 4 h), whereas F-ANANAS-Hz-Dex-M was effective at longer time points.

3.3. *Multiple ANANAS-Hz-Dex-M treatment reduces fibrosis mitigating disease course*

Chronic treatment was conducted using multiple intraperitoneal (i.p.) administrations of free Dex, drug-free ANANAS, and ANANAS-Hz-Dex-M over three weeks (3 injections/week) (Fig. 6). The aim of this study was to evaluate the long-term therapeutic effects of ANANAS-Hz-Dex-M on hepatic inflammation and fibrosis in ARE-Del-/- (HO) male mice.

As illustrated in Fig. 6A, chronic treatment did not induce significant changes in body weight across the different groups at any time points. AMA measurements performed on liver homogenates revealed a significant reduction in antibody levels in HO mice treated with ANANAS-Hz-Dex-M compared with untreated HO mice. Furthermore, a significant decrease in serum ALP levels was observed in the empty ANANAS-

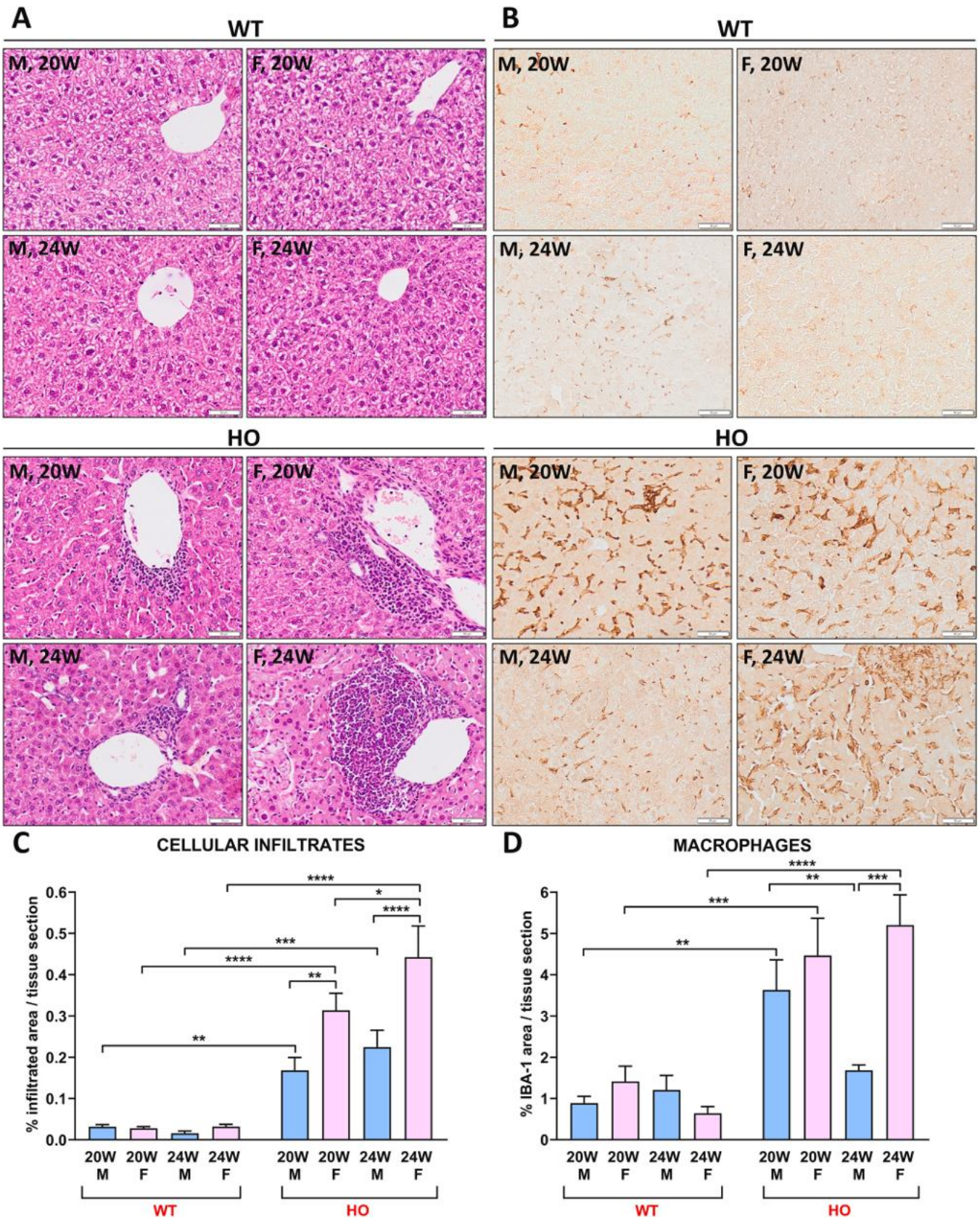

Fig. 2. Liver infiltration assessment. A) HE and B) IBA−1 staining were performed in the livers of males (M) and females (F) ARE-Del WT and HO mice at 20 and 24 weeks of age. Scale bars = 50 μm. Quantification of the area occupied by C) cellular infiltrates and D) macrophages in the whole liver sections was reported. Graph bars show mean + /- SEM (n = 5 for each experimental groups); one-way ANOVA followed by Fisher's LSD test was carried out. Outliers were excluded based on Grubbs' test. *p < 0,05; **p < 0,01; ***p < 0,001; ****p < 0,0001.

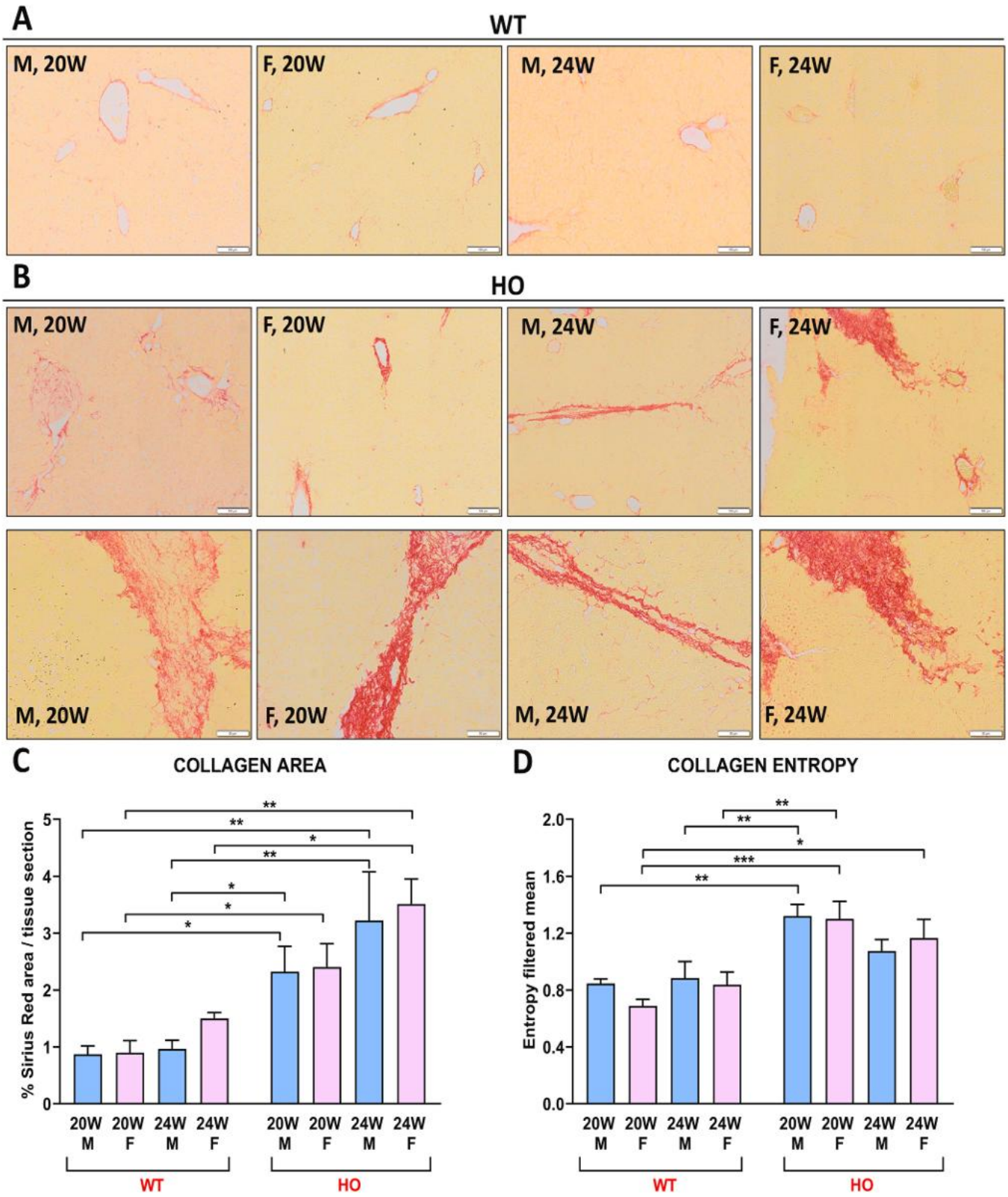

Fig. 3. Liver fibrosis assessment. Sirius Red staining was performed in the livers of males (M) and females (F) ARE-Del WT (A) and HO mice (B) at 20 and 24 weeks of age. Scale bars = 100 μm. Higher magnified pictures were included from HO mice (B, lower panel). Scale bars = 50 μm. C) Quantification of the area occupied by collagen fibres in liver sections. D) Quantification of the collagen fibre entropy. Slice borders (corresponding to the Glisson's capsule) were excluded from the analysis. Graph bars show mean + /- SEM (n = 5 for each experimental groups); one-way ANOVA followed by Fisher's LSD test was carried out. Outliers were excluded based on Grubbs' test. *p < 0,05; **p < 0,01; ***p < 0,001.

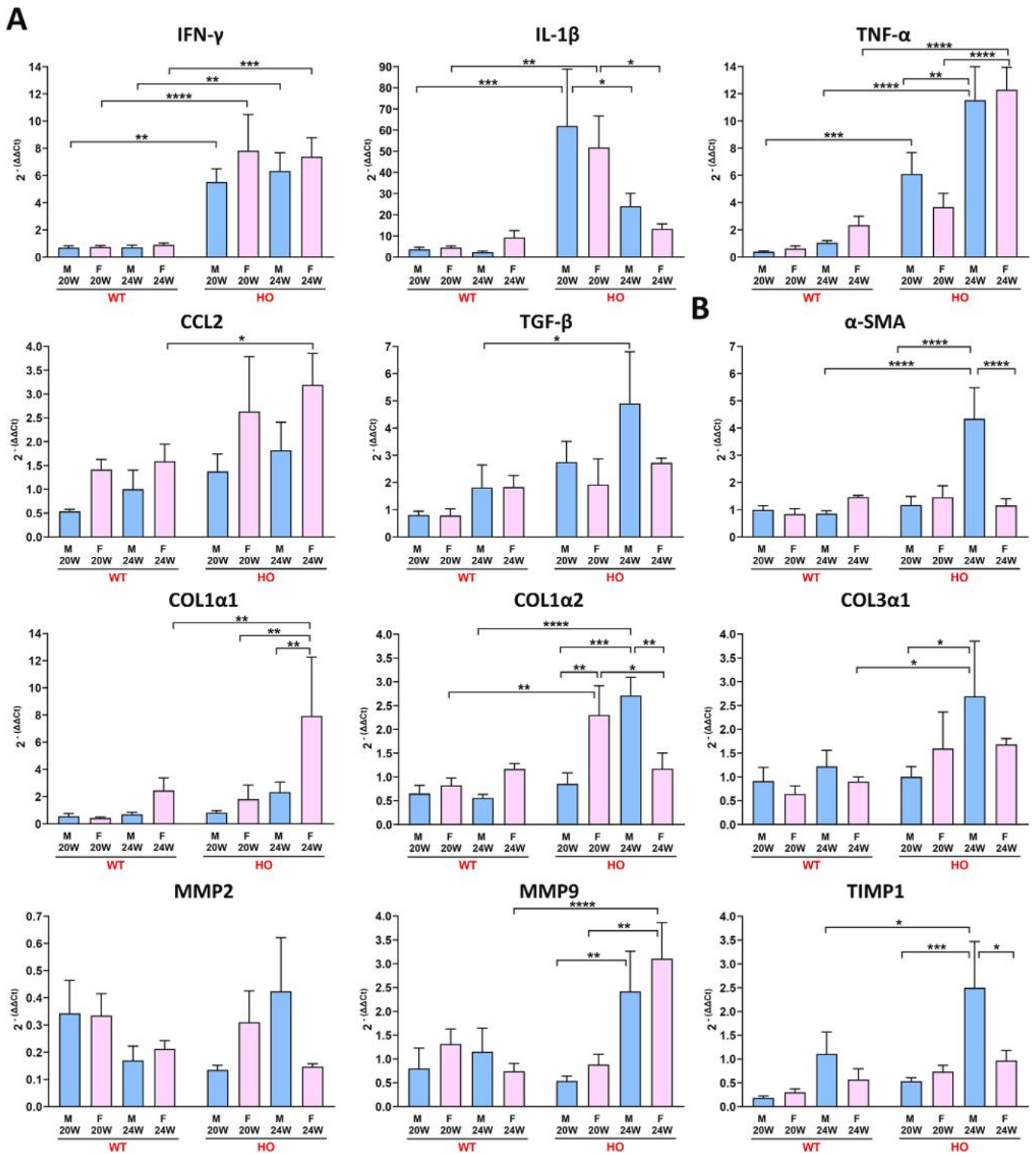

Fig. 4. Relative mRNA expression of inflammatory and fibrotic mediators. Real-time PCR analysis of A) IFN-γ, IL-1β, TNF-α, CCL2, and TGF-β genes; B) α-SMA, COL1α1, COL1α2, COL3α1, MMP2, MMP9, and TIMP1 genes from livers of ARE-Del WT and HO mice at 20 and 24 weeks of age. Graph bars show mean + /- SEM (n = 5 for each experimental groups); one-way ANOVA followed by Fisher's LSD test was carried out. Outliers were excluded based on Grubbs' test. *p < 0,05; **p < 0,01; ***p < 0,001; ****p < 0,0001.

treated group compared with the untreated HO group, although a reduction trend was also noted in the free Dex-treated group. Conversely, both ANANAS and ANANAS-Hz-Dex-M treatments markedly reduced serum TBA levels compared with those observed in untreated HO mice.

Histological analysis of liver sections was used to assess the impact of chronic treatment on hepatic inflammation and fibrosis (Fig. 6B-C). HE staining revealed fewer inflammatory infiltrates only in the Dex-treated group compared to the untreated group. IBA−1 staining revealed no difference in the area occupied by macrophages in whole liver sections between untreated and Dex-treated HO mice. However, a significant increase was measured after chronic treatment with ANANAS or

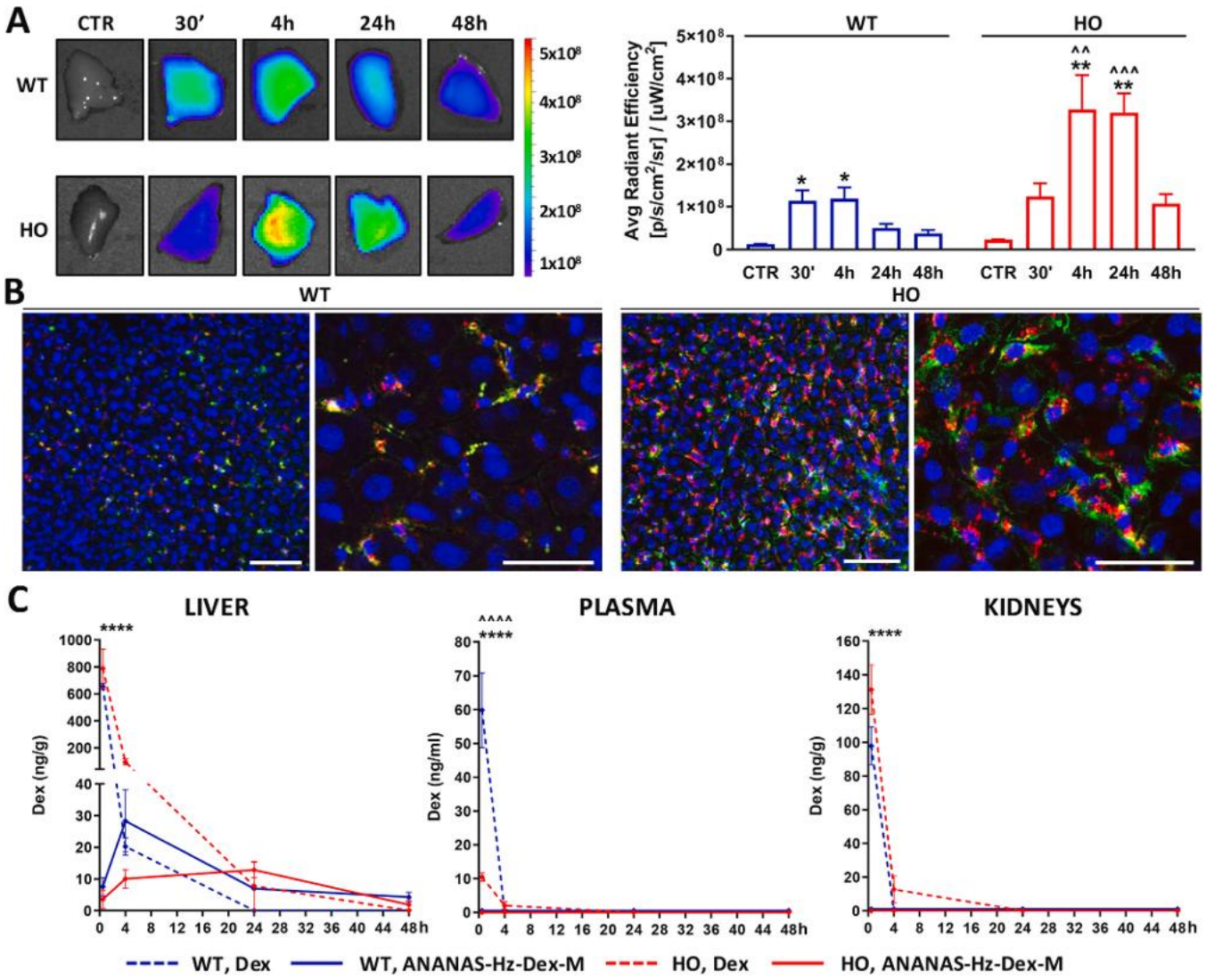

Fig. 5. Nanoformulation biodistribution and pharmacokinetics. A) *Ex vivo* optical imaging of livers from WT and HO mice sacrificed at 30 min, 4, 24 and 48 h after ANANAS-Hz-Dex-M i.p. administration (left panel), correlated with fluorescent signal quantification (right panel). Data are reported as mean + /- SEM. Statistical analysis was performed by One-way ANOVA, followed by Tukey post-hoc test. *= comparison between ANANAS-Hz-Dex-M-treated and untreated mice (CTR). *p < 0.1; **p < 0.01. ^= comparison between livers from WT and HO mice, at the same time point. ^^p < 0.01; ^^^p < 0.001. B) Representative liver images from WT and HO mice sacrificed 4 h after i.p. ANANAS-Hz-Dex-M administration. The blue signal refers to the nuclei (Hoechst−33258 staining), green corresponds to the lysosomal component of macrophages (CD68 Antibody), red is associated with the alexa633 dye linked to the NPs. Scale bars: lower magnified pictures: 100 μm, higher magnified pictures: 50 μm. C) Levels of free Dex measured in liver, plasma and kidneys from WT (blue lines) and HO (red lines) mice. Mice were sacrificed at different time points after i.p. administration of Dex (dotted lines) or ANANAS-Hz-Dex-M (solid lines). Data are reported as mean + /- SEM. Statistical analysis was performed by One-way ANOVA, followed by Tukey post-hoc test. *= comparison between ANANAS-Hz-Dex-M and Dex-treated mice at the same time point. ****p < 0.0001. ^= comparison between free Dex from WT and HO mice, at the same time point. ^^^^p < 0.0001.

ANANAS-Hz-Dex-M. These data were further supported by the measurement of single macrophage size (μm^2) and Feret diameter (μm), which increased after chronic treatment with ANANAS or ANANAS-Hz-Dex-M. The maximum diameter registered for untreated mice was 16 μm, whereas it was 20 μm in NP-treated mice (data not shown), indicating active NP phagocytosis [38]. Interestingly, this size increase was more pronounced after ANANAS-Hz-Dex-M administration (109 μm^2), than after empty ANANAS (77 μm^2) probably owing to the lipophilic nature of Dex, which favours plasmatic membrane crossing. Sirius Red staining revealed a marked reduction in intraparenchymal collagen in all treatment groups compared with the untreated group, without altering collagen fiber entropy.

Gene expression analysis (Fig. 7) revealed no significant differences in the IL-1β, CCL2, or TGF-β mRNA levels after treatment with Dex, ANANAS, or ANANAS-Hz-Dex-M compared with those in the untreated group (Fig. 7A). INF-γ was significantly upregulated in the ANANAS- and ANANAS-Hz-Dex-M-treated groups compared with both the untreated and Dex-treated groups. TNF-α was significantly downregulated by both ANANAS and ANANAS-Hz-Dex-M, as well as by Dex alone. By contrast, all three treatments (Dex, ANANAS, and ANANAS-Hz-Dex-M) significantly reduced the expression of fibrotic markers (COL1α2, COL3α1, α-SMA, MMP2, MMP9, and TIMP1) compared to untreated HO male mice at 24 weeks of age (Fig. 7B), indicating a stronger effect on fibrosis than on inflammation.

Finally, we investigated the involvement of the NF-kB signaling pathway in KCs, as persistent or dysregulated NF-kB activation has been associated with chronic inflammation, exacerbation of liver injury, and fibrosis in a cell type-dependent manner (Fig. 8).

Immunofluorescence analysis of NF-kB (Fig. 8A) revealed enhanced nuclear translocation of NF-kB in KCs (CD68-positive cells) from HO

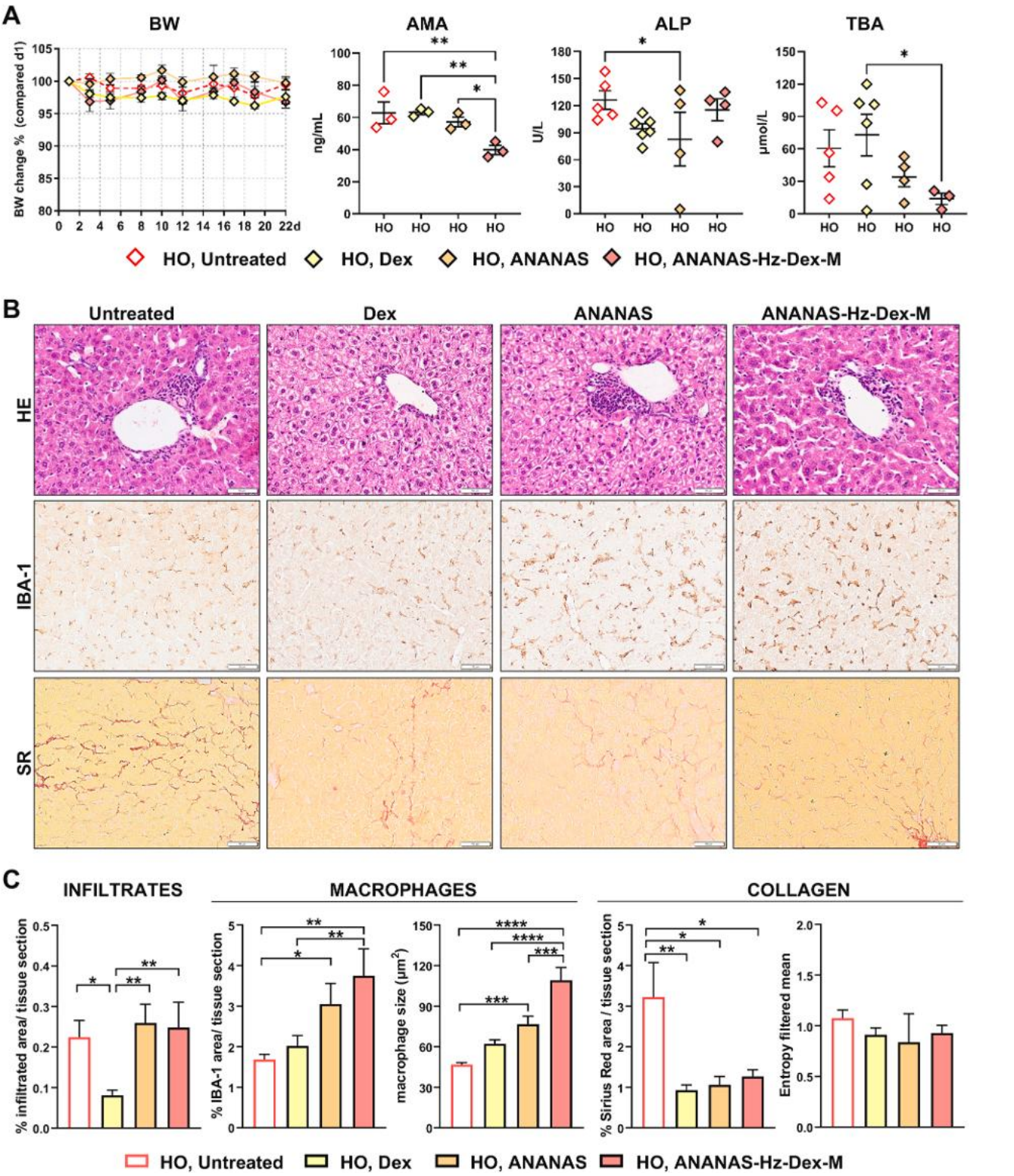

Fig. 6. Serological, biochemical, and histopathological evaluation after chronic treatment. A) body weight, hepatic AMA, serum ALP and serum TBA levels from HO male mice chronically treated with Dex, ANANAS, and ANANAS-Hz-Dex-M. HO untreated experimental group derive from the results reported in Fig. 1 (HO males at 24 w of age), here included again for clarity. Data are presented as a scatter plot, reporting mean + /- SEM. Statistical analysis is performed by One-way ANOVA, followed by Fisher's LSD test. **$p < 0.01$, *$p < 0.1$. B) HE, IBA−1 and SR staining performed in livers from male HO mice untreated or chronically treated with Dex, ANANAS, and ANANAS-Hz-Dex-M. Scale bars = 50 µm. C) Quantification of cellular infiltrates, macrophage area and size, collagen fibers in the whole liver sections, and collagen fiber entropy. Slice borders (corresponding to the Glisson's capsule) were excluded from the analysis of collagen. Graph bars shows mean + /- SEM, One-way ANOVA followed by Fisher's LSD test was carried out. Outliers were excluded on the basis of Grubbs' test. *$p < 0,05$; **$p < 0,01$; ***$p < 0,001$; ****$p < 0,0001$. HO untreated group derive from the results reported in Figs. 2C, 2D, 3C and 3D (HO males at 24 w of age), here included again for clarity.

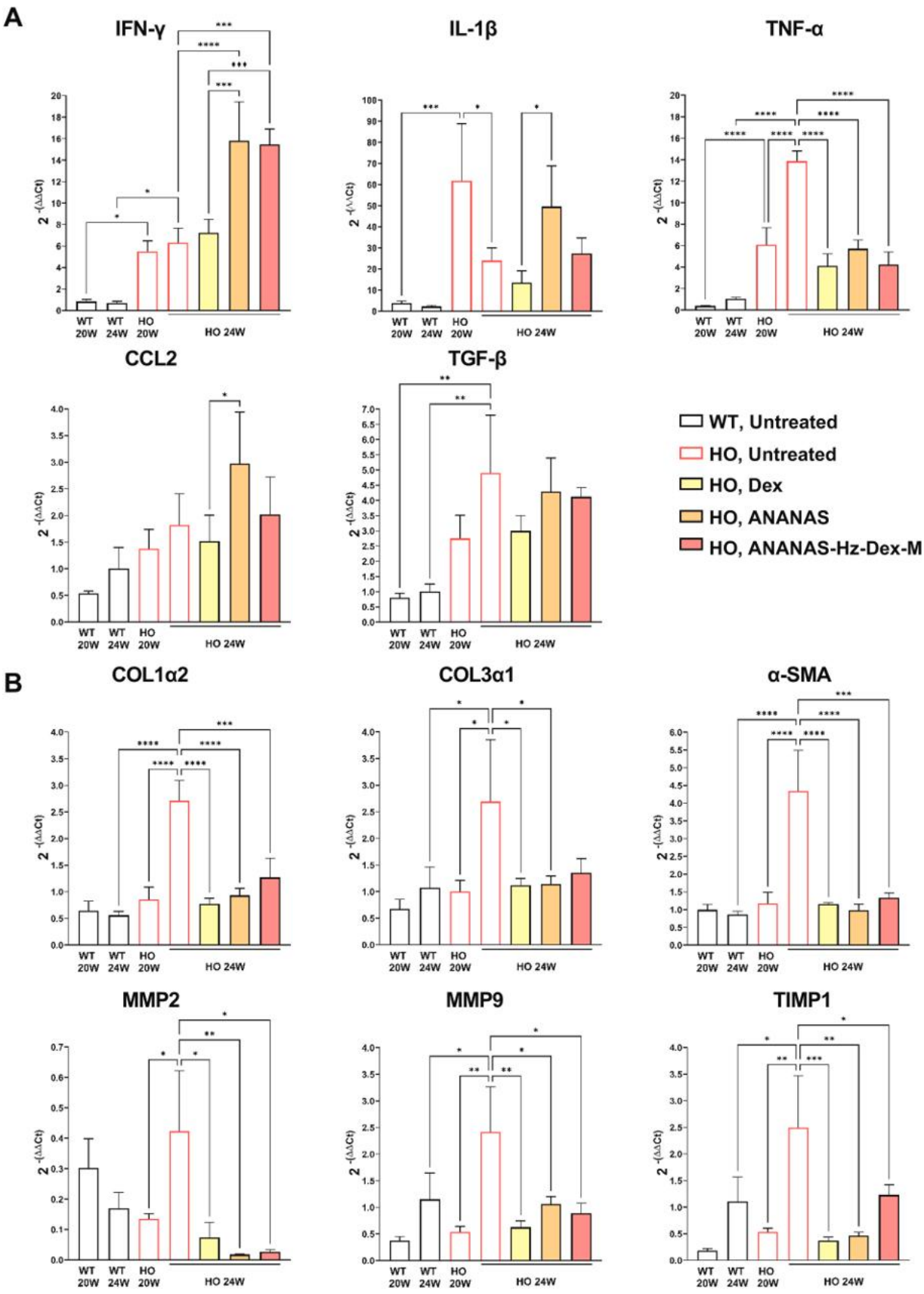

Fig. 7. Relative mRNA expression of inflammatory and fibrotic mediators after chronic treatment. Real-time PCR analysis of A) INF-γ, IL-1β, TNF-α, CCL2, and TGF-β, B) COL1α2, COL3α1, α-SMA, MMP2, MMP9, and TIMP1 genes. HO mice were chronically treated with Dex, ANANAS, and ANANAS-Hz-Dex-M. Untreated WT and HO columns derive from the results reported in Fig. 4, here included again for clarity. Graph bars show means with their relative SEM; One-way ANOVA followed by Fisher's LSD test was carried out. Outliers were excluded based on Grubbs' test. *p < 0,05; **p < 0,01; ***p < 0,001; ****p < 0,0001.

mice compared with WT controls, indicating activation of the pathway. Consistent with these observations, quantification of NF-kB colocalization with KC nuclei (Fig. 8B) showed that ANANAS-Hz-Dex-M treatment, and partially the Dex treatment, reduced its nuclear localization.

3.4. ANANAS-Hz-Dex-M modulate isolated KCs

These findings demonstrate that even empty ANANAS could affect the evolution of liver damage, probably through interactions with macrophages. We thus investigated the effects of NPs on KCs isolated from WT and HO mice and incubated with Dex, ANANAS, or ANANAS-Hz-Dex-M (Fig. 9). The expression of proinflammatory cytokines was markedly increased in HO untreated KCs compared to controls, reflecting the inflammatory state. Treatment with ANANAS-Hz-Dex-M significantly reduced cytokine levels, comparable to Dex alone, highlighting its strong anti-inflammatory potential. We detected a significant reduction in TNF-α in response to Dex and ANANAS-Hz-Dex-M, but also in response to empty ANANAS. TGF-β was moderately upregulated in untreated HO cells, and ANANAS-Hz-Dex-M and Dex treatments effectively attenuated its expression, indicating their capacity to modulate fibrosis. The expression of MMP9, which is involved in ECM remodeling, was downregulated in HO, and this effect was further increased by free Dex and empty ANANAS treatment. The reduction in the analysed parameters induced by empty NPs suggests that the effect observed *in vivo* is also due to the ability of empty ANANAS to affect the macrophage phenotype.

4. Discussion

PBC is a cholestatic disease characterised by chronic autoimmune damage of the biliary tree. Ursodeoxycholic acid (UDCA) is the only approved treatment for PBC, however, a subgroup of patients does not adequately respond to it, presenting a significant challenge in managing PBC. Drug combinations and emerging drugs such as fibrates, or FXR agonists represent a possibility for UDCA-resistant cholestasis; in PBC patients with AIH variant (i.e. overlap PBC-AIH), a combination of UDCA and corticosteroids is typically used [39], but steroid-based therapies require new approaches to minimize common side effects.

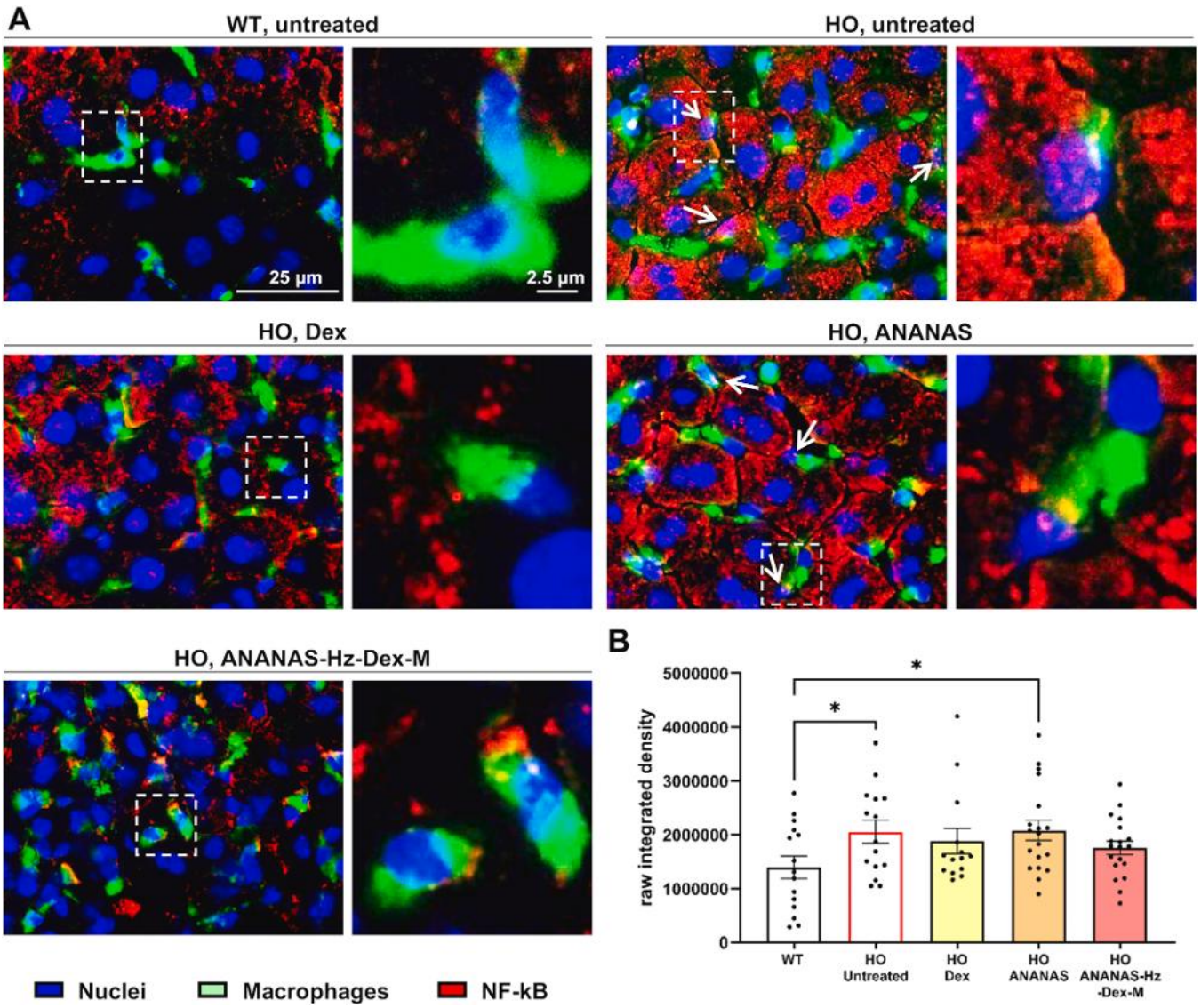

Fig. 8. NF-kB cellular localization. A) Immunohistochemical staining for NF-kB p65 was performed on liver sections from WT and HO (untreated and chronically treated with Dex, ANANAS, and ANANAS-Hz-Dex-M) male mice. NF-kB signal is visible in red, while CD68-positive macrophages are in green. Nuclei are in blue. Two different magnifications are shown, scale bars 25 µm in the lower magnification and 2.5 µm in the insert. B) The histogram shows the fluorescence intensity of nuclear NF-kB, expressed as raw integrated density. Four fields of view per mouse (n = 4) were acquired. Data are presented as mean ± SEM. Statistical analysis was performed using one-way ANOVA followed by Fisher's LSD post hoc test. *$p < 0.05$.

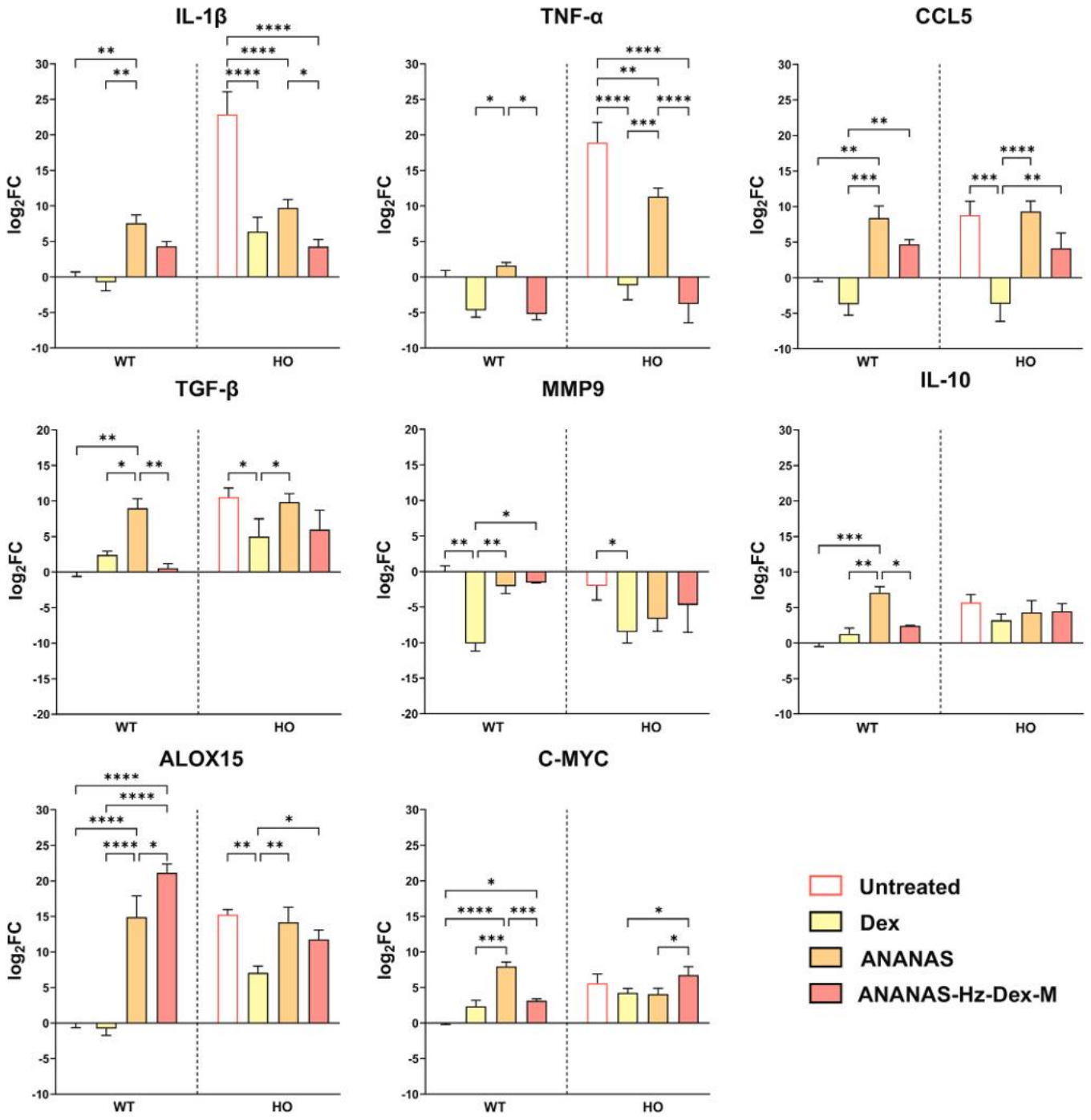

Fig. 9. *In vitro* Kupffer cells treatment. KCs were isolated from the livers of WT and HO mice at 24 w of age. Adherent KCs were treated with either vehicle, Dex (3.17 μg/mL), ANANAS (200 μg/mL), or ANANAS-Hz-Dex at equivalent ANANAS and Dex concentrations in completed DMEM containing 50 ng/mL M-CSF for 24 h. Following the incubation period, cells were harvested for gene expression analysis. Data are presented as mean + SEM (n = 3). Statistical significance was assessed using two-way ANOVA with Tukey post-hoc test. *p < 0.05, **p < 0.01, ***p < 0.001, ****p < 0.0001).

In this context, the use of nanocarriers could be helpful, and our previous studies in a murine model of AIH suggested that dexamethasone-loaded ANANAS are taken up by macrophages and are effective in reducing the expression of liver inflammation markers [19]. This specific localization could be quite important, since the role of cells of the innate immune system is currently becoming pivotal, also modulating the activation of T and natural killer cells [20,21,40]. In addition, macrophages can significantly influence cholangiocyte injury and fibrotic progression [41].

For this study, we exploited the ARE-Del-/- mouse model [23,42,43], characterized by the chronic expression of INF-γ due to the deletion of the 3′ untranslated region of the ARE element, which mimics several key aspects of human PBC pathology. ARE-Del-/- mice presented elevated serum levels of ALP and TBA, together with hepatic portal inflammation and "bridging fibrosis". In this model, the administration of ANANAS carrying dexamethasone led to a reduction in serum TBA levels, AMA levels in liver homogenates, hepatic fibrotic damage, and partially the inflammatory response. Moreover, in non-parenchymal cells, such as KCs, ANANAS-Hz-Dex-M attenuated the activation of NF-kB, a key transcriptional factor driving the inflammatory response, with an

essential role in the regulation of inflammatory signalling pathways in the liver. It is interesting to note that a reduction in NF-κB has also been reported to regulate macrophage polarization and inflammation in both a PBC model and macrophage cell lines [44,45].

Liver-resident macrophages (Kupffer cells) under normal conditions are involved in liver maintenance, but they are activated in the presence of inflammation, as they can also recruit bone marrow-derived monocytes that differentiate into macrophages. From a functional point of view, macrophages can be polarized into M1 and M2 phenotypes due to the presence of different molecules in the external milieu, namely LPS and IFN-γ for M1 polarization and Il-4, IL-10, TGF-β or IL-13 for M2 polarization [46]. In general, M1 macrophages considered proinflammatory and secrete IL-1β, Il-6, and IL-23, whereas M2 macrophages produce different cytokines, have various functions and are divided into M2a, M2b, M2c, and M2d subtypes [46]. In reality, recent data obtained by single-cell analysis on liver tissue showed the presence of ten different macrophage subtypes [47], with an increase in activated macrophages in PBC patients. Other data, obtained by single-cell sequencing, revealed an increase in the IL-1 signalling pathway between KCs and stellate cells in PBC [21], thus supporting the role of macrophages in PBC pathogenesis. Moreover, patients with PBC exhibit elevated levels of monocyte–macrophage precursors in peripheral blood [48], which positively correlate with markers of hepatic injury, as well as increased IL-23 positive macrophage accumulation around bile ducts in hepatic tissues, exacerbating cholangiocyte injury [49]. Macrophage importance is also demonstrated in murine models of PBC, in which KCs regulate NK cells through the secretion of cytokines [20,50].

To evaluate the effect of ANANAS on liver macrophages, we isolated KCs that were treated with ANANAS (empty or loaded with dexamethasone); this treatment was able to reduce the expression of cytokines produced by M1 macrophages, such as Il-1β, TNF-α and CCL5. These data obtained from isolated KCs, although descriptive, are in agreement with those observed on the whole tissue, suggesting that the ANANAS effect could be mediated by a decrease in macrophage proinflammatory cytokine production which, in turn, stimulates stellate and NK cells.

NPs have been demonstrated able to dampen the M1 phenotype or induce a phenotype shift, an effect mainly demonstrated with loaded NPs [51]. Furthermore, our research group has recently demonstrated that glycosylated gold NPs selectively target CD206-expressing M2 macrophages, thereby reducing M1 macrophage infiltration, promoting M2 polarization, and attenuating periductal inflammation and fibrosis in Are-Del-/- mouse models [27].

It must be noted that, in our experimental settings, empty ANANAS treatment was also associated with reduced hepatic fibrosis at histological levels along with decreased mRNA expression of TNF-α and collagens, α-SMA and MMPs, as well as reduced cytokine production. We can hypothesize that the therapeutic effect of these NPs can be due to their interaction with hepatic macrophages, as suggested by the increase in macrophage dimensions due to the substantial uptake of the nanocarrier in their lysosomal compartments. Although this hypothesis needs further experimental evaluations, it has been reported that macrophage engulfment (in this case due to apoptotic bodies) [52], can lead to immunotolerance. Interestingly, this idea was exploited by Kraynak et al. [53], who were able to design nanoparticles with a PLGA core covered by membrane vesicles and an external layer of PEG, which dampened macrophage cytokine production.

Our results with the ANANAS formulation support the efficacy of this nanotherapeutic approach and confirm that resident liver macrophage as a drug target. A promising future application could include not only the use of steroids, but also other drugs (alone or in combination) loaded on such nanoassemblies targeting the pathogenic mechanisms of PBC.

Abbreviations

AIH: autoimmune hepatitis; ALP: alkaline phosphatase; AMA: antimitochondrial antibody; ANANAS: avidin-nucleic-acids-nanoassemblies; ARE-Del: adenylate-uridylate rich element - deletion; CCL2: C-C motif chemokine ligand 2; COL: collagen; Dex: dexamethasone; EHAD: extrahepatic autoimmune diseases; HE: hematoxylin and eosin; HO: homozygous; Hz: hydrazone; IBA−1: ionized calcium-binding adaptor molecule 1; IL: interleukin; IFN-γ: interferon-gamma; KC: Kupffer cells; LSEC: liver sinusoidal endothelial cells; MMP: matrix metalloproteinase; NPs: nanoparticles; PBC: primary biliary cholangitis; PDGF: platelet-derived growth factor; α-SMA: alpha-smooth muscle actin; TBA: total bile acids; TGF: transforming growth factor; TNF: tumor necrosis factor; UDCA: ursodeoxycholic acid; WT: wild-type.

CRediT authorship contribution statement

Paolo Bigini: Supervision, Funding acquisition, Conceptualization. **Marco Carbone:** Writing – review & editing, Funding acquisition, Conceptualization. **Pietro Invernizzi:** Supervision, Funding acquisition. **Sara Pelucchi:** Methodology, Investigation. **Massimiliano Cadamuro:** Methodology, Investigation. **Martina Bruna Violatto:** Writing – original draft, Visualization, Methodology, Investigation, Conceptualization. **Annalisa Morelli:** Methodology, Investigation. **Margherita Morpurgo:** Writing – review & editing, Supervision, Funding acquisition, Conceptualization. **Martina Cattaneo:** Methodology, Investigation. **Elisa Schiavon:** Methodology, Investigation. **Chiara Caime:** Methodology, Investigation. **Manuela Vitulo:** Writing – original draft, Methodology, Investigation. **Simone Bernardotto:** Methodology, Investigation. **Domenico Cerullo:** Methodology, Investigation. **Laura Sironi:** Formal analysis. **Martina Stocco:** Methodology, Investigation. **Stefano Fumagalli:** Formal analysis. **Davide Panzeri:** Formal analysis. **Donatella Barisani:** Supervision, Funding acquisition, Conceptualization. **Naths Grazia Sukubo:** Writing – review & editing, Methodology, Investigation. **Mara Corti:** Methodology, Investigation. **Alessio Gerussi:** Conceptualization. **Laura Cristoferi:** Writing – review & editing. **Alice Passoni:** Methodology, Investigation. **Alessia Lanno:** Methodology, Investigation. **Giulia Yuri Moscatiello:** Methodology, Investigation. **Alessandro Enrico Galbussera:** Methodology, Investigation.

Financial support

This study was supported by Italian Ministry of Health grant (GR-2018-12367794).

Declaration of Competing Interest

The authors declare that they have no known competing financial interests or personal relationships that could have appeared to influence the work reported in this paper.

Appendix A. Supporting information

Supplementary data associated with this article can be found in the online version at doi:10.1016/j.biopha.2026.119770.

Data Availability

Data will be made available on request.

References

[1] A.F. Gulamhusein, G.M. Hirschfield, Primary biliary cholangitis: pathogenesis and therapeutic opportunities, Nat. Rev. Gastroenterol. Hepatol. 17 (2020) 93–110, https://doi.org/10.1038/s41575-019-0226-7.

[2] K.D. Lindor, C.L. Bowlus, J. Boyer, C. Levy, M. Mayo, Primary biliary cholangitis: 2021 practice guidance update from the American Association for the Study of Liver Diseases, Hepatology 75 (2022) 1012–1013, https://doi.org/10.1002/hep.32117.

[3] European Association for the Study of the Liver. Electronic address: easloffice@easloffice.eu, European Association for the Study of the Liver, EASL Clinical Practice Guidelines: The diagnosis and management of patients with primary

biliary cholangitis, J Hepatol 67 (2017) 145–172. https://doi.org/10.1016/j.jhep.2017.03.022.
[4] M.C. van Hooff, E. Werner, A.J. van der Meer, Treatment in primary biliary cholangitis: Beyond ursodeoxycholic acid, Eur. J. Intern. Med. (2024) S0953620524000372, https://doi.org/10.1016/j.ejim.2024.01.030.
[5] J.M. Schattenberg, A. Pares, K.V. Kowdley, M.A. Heneghan, S. Caldwell, D. Pratt, A. Bonder, G.M. Hirschfield, C. Levy, J. Vierling, D. Jones, A. Tailleux, B. Staels, S. Megnien, R. Hanf, D. Magrez, P. Birman, V. Luketic, A randomized placebo-controlled trial of elafibranor in patients with primary biliary cholangitis and incomplete response to UDCA, J. Hepatol. 74 (2021) 1344–1354, https://doi.org/10.1016/j.jhep.2021.01.013.
[6] G.M. Hirschfield, U. Beuers, L. Kupcinskas, P. Ott, A. Bergquist, M. Färkkilä, M. P. Manns, A. Parés, U. Spengler, M. Stiess, R. Greinwald, M. Pröls, D. Wendum, U. Drebber, R. Poupon, A placebo-controlled randomised trial of budesonide for PBC following an insufficient response to UDCA, J. Hepatol. 74 (2021) 321–329, https://doi.org/10.1016/j.jhep.2020.09.011.
[7] P.-A. Soret, L. Lam, F. Carrat, L. Smets, T. Berg, M. Carbone, P. Invernizzi, V. Leroy, P. Trivedi, N. Cazzagon, C. Weiler-Normann, L. Alric, I. Rosa-Hezode, A. Heurgué, J.-P. Cervoni, J. Dumortier, P. Potier, O. Roux, C. Silvain, C. Bureau, R. Anty, D. Larrey, C. Levy, A. Pares, C. Schramm, F. Nevens, O. Chazouillères, C. Corpechot, Combination of fibrates with obeticholic acid is able to normalise biochemical liver tests in patients with difficult-to-treat primary biliary cholangitis, Aliment. Pharmacol. Ther. 53 (2021) 1138–1146, https://doi.org/10.1111/apt.16336.
[8] D. D'Amato, A. De Vincentis, F. Malinverno, M. Viganò, D. Alvaro, M. Pompili, A. Picciotto, V.P. Palitti, M. Russello, S. Storato, M.G. Pigozzi, V. Calvaruso, E. De Gasperi, A. Lleo, A. Castellaneta, A. Pellicelli, N. Cazzagon, A. Floreani, L. Muratori, S. Fagiuoli, G.A. Niro, V. Feletti, R. Cozzolongo, N. Terreni, M. Marzioni, R. Pellicano, P. Pozzoni, L. Baiocchi, L. Chessa, F. Rosina, G. Bertino, M. Vinci, A. Morgando, E. Vanni, G. Scifo, R. Sacco, M. D'Antò, V. Bellia, R. Boldizzoni, S. Casella, B. Omazzi, G. Poggi, L. Cristoferi, A. Gerussi, V. Ronca, R. Venere, F. Ponziani, M. Cannavò, A. Mussetto, R. Fontana, F. Losito, E. Frazzetto, M. Distefano, F. Colapietro, S. Labanca, G. Marconi, G. Grassi, G. Galati, S.E. O'Donnell, C. Mancuso, G. Mulinacci, A. Palermo, E. Claar, A. Izzi, A. Picardi, P. Invernizzi, M. Carbone, U. Vespasiani-Gentilucci, Italian PBC Registry and the Club Epatologi Ospedalieri (CLEO)/Associazione Italiana Gastroenterologi ed Endoscopisti Digestivi Ospedalieri (AIGO) PBC Study Group, Real. -World Exp. obeticholic Acid. Patients Prim. Biliary cholangitis JHEP Rep. 3 (2021) 100248, https://doi.org/10.1016/j.jhepr.2021.100248.
[9] N. Kerkar, A. Chan, Autoimmune hepatitis, sclerosing cholangitis, and autoimmune sclerosing cholangitis or overlap syndrome, Clin. Liver Dis. 22 (2018) 689–702, https://doi.org/10.1016/j.cld.2018.06.005.
[10] A. Bonder, A. Retana, D.M. Winston, J. Leung, M.M. Kaplan, Prevalence of primary biliary cirrhosis–autoimmune hepatitis overlap syndrome, Clin. Gastroenterol. Hepatol. 9 (2011) 609–612, https://doi.org/10.1016/j.cgh.2011.03.019.
[11] X. Fan, T. Wang, Y. Shen, X. Xi, L. Yang, Underestimated male prevalence of primary biliary cholangitis in China: results of a 16-yr cohort study involving 769 patients, Sci. Rep. 7 (2017) 6560, https://doi.org/10.1038/s41598-017-06807-7.
[12] Y.-Q. Fang, D.-X. Lv, W. Jia, J. Li, Y.-Q. Deng, Y. Wang, M. Yu, G.-Q. Wang, Case–control study on prednisolone combined with ursodeoxycholic acid and azathioprine in pure primary biliary cirrhosis with high levels of immunoglobulin G and transaminases: efficacy and safety analysis, Medicine 93 (2014) e104, https://doi.org/10.1097/MD.0000000000000104.
[13] J.-D. Qian, T.-T. Yao, Y. Wang, G.-Q. Wang, Treatment of primary biliary cholangitis with ursodeoxycholic acid, prednisolone and immunosuppressants in patients not responding to ursodeoxycholic acid alone and the prognostic indicators, Clin. Res. Hepatol. Gastroenterol. 44 (2020) 874–884, https://doi.org/10.1016/j.clinre.2020.03.026.
[14] M.J. Mitchell, M.M. Billingsley, R.M. Haley, M.E. Wechsler, N.A. Peppas, R. Langer, Engineering precision nanoparticles for drug delivery, Nat. Rev. Drug. Discov. 20 (2021) 101–124, https://doi.org/10.1038/s41573-020-0090-8.
[15] Y.-N. Zhang, W. Poon, A.J. Tavares, I.D. McGilvray, W.C.W. Chan, Nanoparticle–liver interactions: cellular uptake and hepatobiliary elimination, J. Control. Release 240 (2016) 332–348, https://doi.org/10.1016/j.jconrel.2016.01.020.
[16] K.M. Tsoi, S.A. MacParland, X.-Z. Ma, V.N. Spetzler, J. Echeverri, B. Ouyang, S. M. Fadel, E.A. Sykes, N. Goldaracena, J.M. Kaths, J.B. Conneely, B.A. Alman, M. Selzner, M.A. Ostrowski, O.A. Adeyi, A. Zilman, I.D. McGilvray, W.C.W. Chan, Mechanism of hard-nanomaterial clearance by the liver, Nat. Mater. 15 (2016) 1212–1221, https://doi.org/10.1038/nmat4718.
[17] J. Li, C. Chen, T. Xia, Understanding nanomaterial-liver interactions to facilitate the development of safer nanoapplications, Adv. Mater. 34 (2022) e2106456, https://doi.org/10.1002/adma.202106456.
[18] P. Bigini, S. Previdi, E. Casarin, D. Silvestri, M.B. Violatto, S. Facchin, L. Sitia, A. Rosato, G. Zuccolotto, N. Realdon, F. Fiordaliso, M. Salmona, M. Morpurgo, In vivo fate of avidin-nucleic acid nanoassemblies as multifunctional diagnostic tools, ACS Nano 8 (2014) 175–187, https://doi.org/10.1021/nn402669w.
[19] M.B. Violatto, E. Casarin, L. Talamini, L. Russo, S. Baldan, C. Tondello, M. Messmer, E. Hintermann, A. Rossi, A. Passoni, R. Bagnati, S. Biffi, C. Toffanin, S. Gimondi, S. Fumagalli, M.-G. De Simoni, D. Barisani, M. Salmona, U. Christen, P. Invernizzi, P. Bigini, M. Morpurgo, Dexamethasone conjugation to biodegradable avidin-nucleic-acid-nano-assemblies promotes selective liver targeting and improves therapeutic efficacy in an autoimmune hepatitis murine model, ACS Nano 13 (2019) 4410–4423, https://doi.org/10.1021/acsnano.8b09655.
[20] H.-Y. Fu, W.-M. Bao, C.-X. Yang, W.-J. Lai, J.-M. Xu, H.-Y. Yu, Y.-N. Yang, X. Tan, A.K. Gupta, Y.-M. Tang, Kupffer Cells Regulate Natural Killer Cells Via the NK group 2, Member D (NKG2D)/Retinoic Acid Early Inducible-1 (RAE-1) Interaction and Cytokines in a Primary Biliary Cholangitis Mouse Model, Med. Sci. Monit. 26 (2020), https://doi.org/10.12659/MSM.923726.
[21] C. Jin, P. Jiang, Z. Zhang, Y. Han, X. Wen, L. Zheng, W. Kuang, J. Lian, G. Yu, X. Qian, Y. Ren, M. Lu, L. Xu, W. Chen, J. Chen, Y. Zhou, J. Xin, B. Wang, X. Jin, P. Qian, Y. Yang, Single-cell RNA sequencing reveals the pro-inflammatory roles of liver-resident Th1-like cells in primary biliary cholangitis, Nat. Commun. 15 (2024) 8690, https://doi.org/10.1038/s41467-024-53104-9.
[22] D.L. Hodge, C. Berthet, V. Coppola, W. Kastenmüller, M.D. Buschman, P. M. Schaughency, H. Shirota, A.J. Scarzello, J.J. Subleski, M.R. Anver, J.R. Ortaldo, F. Lin, D.A. Reynolds, M.E. Sanford, P. Kaldis, L. Tessarollo, D.M. Klinman, H. A. Young, IFN-gamma AU-rich element removal promotes chronic IFN-gamma expression and autoimmunity in mice, J. Autoimmun. 53 (2014) 33–45, https://doi.org/10.1016/j.jaut.2014.02.003.
[23] H.R. Bae, P.S.C. Leung, K. Tsuneyama, J.C. Valencia, D.L. Hodge, S. Kim, T. Back, M. Karwan, A.S. Merchant, N. Baba, D. Feng, O. Park, B. Gao, G.-X. Yang, M. E. Gershwin, H.A. Young, Chronic expression of interferon-gamma leads to murine autoimmune cholangitis with a female predominance, Hepatology 64 (2016) 1189–1201, https://doi.org/10.1002/hep.28641.
[24] A. Morelli, E. Schiavon, M.B. Violatto, G.Y. Moscatiello, A. Salmaso, A. Passoni, A. Lanno, S. Bernardotto, M. Stocco, A. Mattarei, R. Bagnati, F. Meloni, P. Bigini, M. Morpurgo, Dexamethasone conjugation to an Avidin-Nucleic-Acid-NanoASsembly eliminates the steroid plasma absorption, enhancing selective lung tropism in a murine model of pulmonary fibrosis, Drug. Deliv. 32 (2025) 2531063, https://doi.org/10.1080/10717544.2025.2531063.
[25] M. Pignatto, N. Realdon, M. Morpurgo, Optimized avidin nucleic acid nanoassemblies by a tailored PEGylation strategy and their application as molecular amplifiers in detection, Bioconjug Chem. 21 (2010) 1254–1263, https://doi.org/10.1021/bc100044u.
[26] A. Ongaro, M.B. Violatto, E. Casarin, I. Pellerani, G. Marchini, G. Ribaudo, M. Salmona, M. Carbone, A. Passoni, E. Gnodi, E. Schiavon, A. Mattarei, D. Barisani, P. Invernizzi, P. Bigini, M. Morpurgo, The mode of dexamethasone decoration influences avidin-nucleic-acid-nano-assembly organ biodistribution and in vivo drug persistence, Nanomed. Nanotechnol. Biol. Med. 40 (2022) 102497, https://doi.org/10.1016/j.nano.2021.102497.
[27] J. Fernandez Alarcon, P. Perez Schmidt, N. Panini, F. Caruso, M.B. Violatto, N. G. Sukubo, A. Martinez-Serra, C.B. Ekalle-Soppo, A. Morelli, G.Y. Moscatiello, C. Grasselli, A. Corbelli, F. Fiordaliso, J. Kelk, L. Petrosilli, G. d'Orazio, R. Mateu Ferrando, A. Verdaguer Ferrer, C. Fornaguera, L. Lay, S. Fumagalli, S. Recchia, M. P. Monopoli, L. Polito, P. Bigini, G. Sitia, Functional polarization of liver macrophages by glyco gold nanoparticles, Adv. Sci. 12 (2025) 2407458, https://doi.org/10.1002/advs.202407458.
[28] P. Bankhead, M.B. Loughrey, J.A. Fernández, Y. Dombrowski, D.G. McArt, P. D. Dunne, S. McQuaid, R.T. Gray, L.J. Murray, H.G. Coleman, J.A. James, M. Salto-Tellez, P.W. Hamilton, QuPath: open source software for digital pathology image analysis, Sci. Rep. 7 (2017) 16878, https://doi.org/10.1038/s41598-017-17204-5.
[29] R. Akpinar, D. Panzeri, C. De Carlo, V. Belsito, B. Durante, G. Chirico, R. Lombardi, A.L. Fracanzani, M. Maggioni, I. Arcari, M. Roncalli, L.M. Terracciano, D. Inverso, A. Aghemo, N. Pugliese, L. Sironi, L. Di Tommaso, Role of artificial intelligence in staging and assessing of treatment response in MASH patients, Front. Med. 11 (2024) 1480866, https://doi.org/10.3389/fmed.2024.1480866.
[30] F. Andreata, C. Blériot, P. Di Lucia, G. De Simone, V. Fumagalli, X. Ficht, C. G. Beccaria, M. Kuka, F. Ginhoux, M. Iannacone, Isolation of mouse Kupffer cells for phenotypic and functional studies, STAR Protoc. 2 (2021) 100831, https://doi.org/10.1016/j.xpro.2021.100831.
[31] M. Bolognesi, C. Merkel, D. Sacerdoti, V. Nava, A. Gatta, Role of spleen enlargement in cirrhosis with portal hypertension, Dig. Liver Dis. 34 (2002) 144–150, https://doi.org/10.1016/S1590-8658(02)80246-8.
[32] C.-B. Wang, Y. Wang, Y. Yao, J.-J. Wang, K. Tsuneyama, Q. Yang, B. Liu, C. Selmi, M.E. Gershwin, S.-H. Yang, Z.-X. Lian, The gut microbiome contributes to splenomegaly and tissue inflammation in a murine model of primary biliary cholangitis, 507, Ann. Transl. Med. 10 (2022) 507, https://doi.org/10.21037/atm-21-5448.
[33] R.C. de Veer, M.H. Harms, C. Corpechot, D. Thorburn, P. Invernizzi, H.L. A. Janssen, P.M. Battezzati, F. Nevens, K.D. Lindor, A. Floreani, C.Y. Ponsioen, M. J. Mayo, A. Parés, A.L. Mason, K.V. Kowdley, P.J. Trivedi, G.M. Hirschfield, T. Bruns, G.N. Dalekos, N.K. Gatselis, X. Verhelst, W.J. Lammers, B.E. Hansen, H. R. van Buuren, A.J. van der Meer, the Global PBC Study Group, Liver transplant-free survival according to alkaline phosphatase and GLOBE score in patients with primary biliary cholangitis treated with ursodeoxycholic acid, Aliment. Pharmacol. Ther. 56 (2022) 1408–1418, https://doi.org/10.1111/apt.17226.
[34] L. Salvatore, N. Gallo, M.L. Natali, A. Terzi, A. Sannino, M. Madaghiele, Mimicking the hierarchical organization of natural collagen: toward the development of ideal scaffolding material for tissue regeneration, Front. Bioeng. Biotechnol. 9 (2021) 644595, https://doi.org/10.3389/fbioe.2021.644595.
[35] L. Zeldin, G.E. Mosley, D. Laudier, Z.S. Gallate, J. Gansau, R.C. Hoy, J. Poeran, J. C. Iatridis, Spatial mapping of collagen content and structure in human intervertebral disk degeneration, JOR Spine 3 (2020) e1129, https://doi.org/10.1002/jsp2.1129.
[36] S. Koilan, D. Hamilton, N. Baburyan, M.K. Padala, K.T. Weber, R.V. Guntaka, Prevention of liver fibrosis by triple helix-forming oligodeoxyribonucleotides targeted to the promoter region of type I collagen gene, Oligonucleotides 20 (2010) 231–237, https://doi.org/10.1089/oli.2010.0244.

[37] H.-P. Ma, H.-L. Chang, O.A. Bamodu, V.K. Yadav, T.-Y. Huang, A.T.H. Wu, C.-T. Yeh, S.-H. Tsai, W.-H. Lee, Collagen 1A1 (COL1A1) is a reliable biomarker and putative therapeutic target for hepatocellular carcinogenesis and metastasis, Cancers (Basel) 11 (2019) 786, https://doi.org/10.3390/cancers11060786.
[38] L. Bouwens, M. Baekeland, R. de Zanger, E. Wisse, Quantitation, tissue distribution and proliferation kinetics of kupffer cells in normal rat liver, Hepatology 6 (1986) 718–722, https://doi.org/10.1002/hep.1840060430.
[39] B.L. Freedman, C.J. Danford, V. Patwardhan, A. Bonder, Treatment of overlap syndromes in autoimmune liver disease: a systematic review and meta-analysis, JCM 9 (2020) 1449, https://doi.org/10.3390/jcm9051449.
[40] P.-Y. Luo, M. Ma, M.-C. Liu, Y.-H. Wu, J. Long, M.-X. Huang, S.-Y. Yang, T.-T. Da, K. Tsuneyama, Q. Li, H. Jin, Z.-B. Zhao, J. Wang, X. Ma, M.E. Gershwin, Y. Han, Z.-X. Lian, L. Li, Autophagy of Kupffer cells modulates $CD8^+$ T cell activation in primary biliary cholangitis, Gut (2025) gutjnl-2025-335611, https://doi.org/10.1136/gutjnl-2025-335611.
[41] T. Liu, Y. Wang, Y. Huang, R. Zhao, H. Shen, Macrophages in autoimmune liver diseases: from immune homeostasis to precision-targeted therapy, Biomedicines 13 (2025) 2520, https://doi.org/10.3390/biomedicines13102520.
[42] A. Tanaka, P.S.C. Leung, H.A. Young, M.E. Gershwin, Therapeutic and immunological interventions in primary biliary cholangitis: from mouse models to humans, Aoms (2017), https://doi.org/10.5114/aoms.2017.70995.
[43] S. Oertelt, W.M. Ridgway, A.A. Ansari, R.L. Coppel, M.E. Gershwin, Murine models of primary biliary cirrhosis: comparisons and contrasts, Hepatol. Res. 37 (2007), https://doi.org/10.1111/j.1872-034X.2007.00226.x.
[44] G.M. Gallucci, B. Alsuwayt, A.M. Auclair, J.L. Boyer, D.N. Assis, N.S. Ghonem, Fenofibrate downregulates NF-κB signaling to inhibit pro-inflammatory cytokine secretion in human THP-1 macrophages and during primary biliary cholangitis, Inflammation 45 (2022) 2570–2581, https://doi.org/10.1007/s10753-022-01713-1.
[45] Z. Wang, W. Gao, X. Cheng, N. Zhang, W. Lu, Y. Li, M. Liu, Vitamin D3 attenuates hepatic inflammation in primary biliary cholangitis by inhibiting TLR4/NF-κB mediated M1 macrophage polarization, Sci. Rep. 15 (2025) 44345, https://doi.org/10.1038/s41598-025-27911-z.
[46] C. Wang, C. Ma, L. Gong, Y. Guo, K. Fu, Y. Zhang, H. Zhou, Y. Li, Macrophage polarization and its role in liver disease, Front. Immunol. 12 (2021) 803037, https://doi.org/10.3389/fimmu.2021.803037.
[47] T.S. Andrews, D. Nakib, C.T. Perciani, X.Z. Ma, L. Liu, E. Winter, D. Camat, S. W. Chung, P. Lumanto, J. Manuel, S. Mangroo, B. Hansen, B. Arpinder, C. Thoeni, B. Sayed, J. Feld, A. Gehring, A. Gulamhusein, G.M. Hirschfield, A. Ricciuto, G. D. Bader, I.D. McGilvray, S. MacParland, Single-cell, single-nucleus, and spatial transcriptomics characterization of the immunological landscape in the healthy and PSC human liver, J. Hepatol. 80 (2024) 730–743, https://doi.org/10.1016/j.jhep.2023.12.023.
[48] A. Peng, P. Ke, R. Zhao, X. Lu, C. Zhang, X. Huang, G. Tian, J. Huang, J. Wang, P. Invernizzi, Q. Chen, J. Zhuang, Elevated circulating CD14lowCD16+ monocyte subset in primary biliary cirrhosis correlates with liver injury and promotes Th1 polarization, Clin. Exp. Med. 16 (2016) 511–521, https://doi.org/10.1007/s10238-015-0381-2.
[49] C.-Y. Yang, X. Ma, K. Tsuneyama, S. Huang, T. Takahashi, N.P. Chalasani, C. L. Bowlus, G.-X. Yang, P.S.C. Leung, A.A. Ansari, L. Wu, R.L. Coppel, E. M. Gershwin, IL-12/Th1 and IL-23/Th17 biliary microenvironment in primary biliary cirrhosis: implications for therapy, Hepatology 59 (2014) 1944–1953, https://doi.org/10.1002/hep.26979.
[50] D. Reuveni, M.R. Brezis, E. Brazowski, P. Vinestock, P.S.C. Leung, P. Thakker, M. E. Gershwin, E. Zigmond, Interleukin 23 produced by hepatic monocyte-derived macrophages is essential for the development of murine primary biliary cholangitis, Front. Immunol. 12 (2021) 718841, https://doi.org/10.3389/fimmu.2021.718841.
[51] M.M. Alvarez, J.C. Liu, G. Trujillo-de Santiago, B.-H. Cha, A. Vishwakarma, A. M. Ghaemmaghami, A. Khademhosseini, Delivery strategies to control inflammatory response: modulating M1–M2 polarization in tissue engineering applications, J. Control. Release 240 (2016) 349–363, https://doi.org/10.1016/j.jconrel.2016.01.026.
[52] Y. Peng, D.A. Martin, J. Kenkel, K. Zhang, C.A. Ogden, K.B. Elkon, Innate and adaptive immune response to apoptotic cells, J. Autoimmun. 29 (2007) 303–309, https://doi.org/10.1016/j.jaut.2007.07.017.
[53] C.A. Kraynak, W. Huang, E.C. Bender, J.-L. Wang, M.S. Hanafy, Z. Cui, L.J. Suggs, Apoptotic body-inspired nanoparticles target macrophages at sites of inflammation to support an anti-inflammatory phenotype shift, Int. J. Pharm. 618 (2022) 121634, https://doi.org/10.1016/j.ijpharm.2022.121634.